Robust Control and System Identification for Flexible Structures

A THESIS

SUBMITTED TO THE FACULTY OF THE GRADUATE SCHOOL

OF THE UNIVERSITY OF MINNESOTA

BY

Volkan Nalbantoğlu

IN PARTIAL FULFILLMENT OF THE REQUIREMENTS

FOR THE DEGREE OF

DOCTOR OF PHILOSOPHY

Gary J. Balas, Adviser

July 1998

UNIVERSITY OF MINNESOTA

This is to certify that I have examined this copy of a doctoral thesis by

Volkan Nalbantoğlu

and have found that it is complete and satisfactory in all respects,
and that any and all revisions required by the final
examining committee have been made.

Gary J. Balas

Name of Faculty Adviser

Signature of Faculty Adviser

Date

GRADUATE SCHOOL

Acknowledgments

I would like to thank my advisor Gary Balas for his support, encouragement and patience during my stay at the University of Minnesota. He always provided original research ideas and an excellent environment and guidance for realizing them. It was a great pleasure to work with him. I would like to thank Dr. Jozsef Bokor for inviting me to the Computer and Automation Research institute of the Hungarian Academy of Sciences and introducing me to the field of system identification. I am also thankful to my exam committee members, Dr. Zhao, Dr. Georgiou, Dr. Leo and Dr. Lee.

The friends at Room 15 have been the source of great motivation and fun. Thanks to Peter, Arun, Rick, Jeff, Jim, JY, Jack and Raktim. I will miss the conversations we had, the bike rides and the volleyball and football games on short Minnesota summers. I especially would like to thank Rick for his collaboration and initiations on common research areas. Also thanks to Jim and Greg for making it fun to work on "mysterious" experimental problems that we had with the structure.

The Turkish community and my roommates, Joe and Julio, have been very supportive during my stay in Minnesota. I would like to thank them for their friendship and reminding me that I should finish some day! Special thanks to the neighbors, Cetin, Bayram and Mehmet.

Finally, it is a pleasure for me to thank my family for their understanding and encouragement in following my ideals.

Abstract

System identification and sensor type selection and placement problems are examined for flexible structures in this thesis. System identification with generalized orthonormal basis functions prove to be suitable for modeling flexible structures. Generalized orthonormal functions allow for the incorporation of a-priori information about the system into the identification process in the form of approximate pole locations. It is shown that specifying the pole location at the beginning of the identification process leads to a low order minimal multivariable realization for flexible structures. It is observed that the system poles play an important role in the accuracy of the model, therefore a method for refining the pole locations is developed.

In a control design problem, the performance requirements and feedback signals are usually assumed to be given. However, for flexible structures, due to the order of the structural model and limited effectiveness of the lumped sensors and actuators, the performance requirements and optimum location for sensors are not obvious. Hence defining the objectives of active control is an important part of control design. In this thesis the role of performance criteria selection for vibration attenuation of flexible structures is investigated. It is shown that using non-collocated acceleration feedback has advantages over collocated displacement and velocity feedback when the performance objective is vibration attenuation. A natural extension of choosing performance requirements and feedback signal types is the optimal placement of sensors. A technique based on full control synthesis is developed for finding the optimal sensor locations. An experimental four story flexible structure is used to test the results. Experimental results show that the sensor locations based on full control synthesis are effective for output control design.

Contents

List of Figures

List of Tables

List of Symbols

$\mathbf{R}$	Field of real numbers
$\mathbf{R}^n$	Field of vectors with n real elements
$\mathbf{R}^{n\times m}$	Field of real matrices with n rows and m columns
$\mathbf{C}$	Field of complex numbers
$\mathbf{C}^n$	Field of vectors with n complex elements
$\mathbf{C}^{n\times m}$	Field of complex matrices with n rows and m columns
A^T	Transpose of matrix or vector A
A^*	Complex conjugate transpose of matrix or vector A
$\sigma(M)$	Singular value of matrix M
$\overline{\sigma}(M)$	Maximum singular value of matrix M
$\rho(M)$	Spectral radius of matrix M
$\lambda(M)$	Eigenvalue of matrix M
Tr(M)	Trace of a square matrix M
det(M)	Determinant of a square matrix M
Re(M)	Real part of a square matrix M
Im(M)	Imaginary part of a square matrix M
I_n	Identity matrix of size $n \times n$
s	Variable of the Laplace transform
z	Variable of the z-transform
$H_2^\perp$	The Hardy space of functions analytical outside the unit disc with quadratic norm.
H_2	The Hardy space of functions analytical inside the unit disc with quadratic norm.
l_2	Space of square summable sequences
dimH	The dimension of a space H.
$A \ominus B$	Orthogonal complement of B to A.

$\langle ., . \rangle$	Scalar product.

Chapter 1

Introduction

Lightly damped, flexible structures are an interesting and challenging field of application for robust control and system identification. Future space stations, tall buildings under earthquake and wind loading, large civil engineering machinery are some of the examples of flexible structures that require active control for safe and precise operation.

Closely spaced, lightly damped modes of these structures make the accurate modeling and control a difficult task. For practical control design, the models of these systems should not be very complex, and modeling errors in the natural frequencies and damping levels of the controlled modes and unmodeled high frequency modes should be taken into account in the control design process.

In the last two decades there has been substantial research in modeling and control of flexible structures. The main part of this research was concerned with applying new digital technology and multi-input/multi-output (MIMO) robust control design techniques to flexible structures [2, 5, 8, 24, 10, 20]. Using smart materials such as shape memory alloys and magnetorheological fluids as passive damping elements to augment active control is also a growing area of research [48, 43].

Having an accurate model is an essential step in design of a high performance active control system. This model may be obtained from first principles, finite element modeling or system identification. System identification is a method for constructing a mathematical model for a dynamical system from input-output data. For complex systems it provides a valuable alternative to modeling from fundamental laws of physics. Experimental results show that the modeling of large flexible structures via finite element method may not be accurate enough for high performance active control design purposes [2].

There are a large variety of system identification techniques for dynamical systems [32, 37, 24, 21]. However most of these techniques are not well suited to modeling flexible structures due to the complexity of these systems. Some researchers have specifically tailored system identification algorithms to identify flexible systems. In [9], Bayard develops a technique for curve fitting nonparametric frequency domain data to identify a parametric model composed of two models in parallel, where each model has dynamics in a specified portion of the frequency band. In [4] Balas and Doyle use Chebyshev polynomials to fit the single-input/multi-output experimental frequency domain data ([14]) and an ad hoc model reduction technique based on a-priori knowledge of the system and singular value decomposition to develop a multivariable model. In [24] Juang develops a system identification technique specific for large flexible structures. Markov parameters (sampled pulse or impulse response) of the system to be identified is calculated from time or frequency domain experimental data and a multi-input/multi-output (MIMO) state space model and an observer are constructed from the Markov parameters. Gilpin *etal.* in [20] present a method of obtaining a uniquely identifiable, multi-input/multi-output model which avoids the need for a model reduction algorithm. The state space model is constructed from the matrix partial fraction expansion of the system transfer function matrix by using a dyadic decomposition of the matrix partial fraction expansion residue matrices.

The above system identification techniques represent the model in the canonical basis $\{z^{-k}, k = 0, 1, ...\}$, where z^{-1} is a delay operator. An alternative to representing a system model in canonical basis is to represent the system model in terms of the orthonormal basis generated by the a-priori information about the poles of the system [22, 36, 49, 19]. In the first part of this thesis the application of system identification technique using orthonormal basis functions to flexible structures is examined. System identification with orthonormal functions allow the introduction of a-priori information about the system poles into the system identification process. It is shown on an experimental structure that this provides advantages for identifying MIMO models for flexible structures. However this approach is sensitive to the accuracy of the pole locations, therefore a ad-hoc method is developed for refining the pole locations.

In a control design problem, the performance requirements and feedback signals are usually assumed to be given. However, for flexible structures, due to the state order of the plant model and limited effectiveness of the lumped sensors and actuators, the performance requirements and feedback signal types are not obvious. Hence defining the objectives of active control is an important part of control design. In this thesis the role of performance criteria selection for vibration attenuation of flexible structures is investigated. Defining the "correct" performance objective is key to designing a good controller.

For flexible structures there usually is a freedom in choosing sensor and actuator locations. A systematic way of finding the optimal sensor locations for accurate and economic control design becomes an interesting engineering problem. The second part of the thesis examines the actuator and sensor placement problem for flexible structures.

One approach to the selection of sensor locations is to consider a cost function which includes the observability grammians in minimizing a cost function. Skelton and DeLorenzo consider a cost function as an LQG performance metric formulated as the root mean square contribution of each sensor output. Sensors associated with small cost functions may be removed due to their low effectiveness [42]. Similar approaches are developed using modal properties. Kim and Jenkins choose a performance metric based on modal controllability weighted by the modal cost of Skelton [26]. This approach emphasizes both the degree of controllability and modal participation in the performance criteria. An alternative approach by Lim involves the relationship between grammian singular values and modal observability [27]. The performance metric is a weighted modal projection with actuator and sensor pairs chosen such that principal directions are parallel to the modes with large singular values. In [7] Balas and Young develop a sensor selection technique that takes into account the closed-loop performance objectives. Different sensor locations are compared based on the information each group of sensors can observe. The information is quantified in terms of the associated H_2 cost of estimating the full system state.

The technique presented in this thesis considers a set of candidate sensor locations. Globally optimal, Full Control H_∞ based compensators are computed at each of these locations to determine the maximum performance and robustness level achievable. The sensor locations chosen for implementation on the physical system correspond to the sensor locations achieving the best Full Control H_∞ performance. There is no guarantee that the optimal Full Control sensor locations are equivalent to the optimal sensor locations for a general output feedback controller; however, experiments indicate this technique can choose effective configurations for a physical system. In this technique it is possible to include the system uncertainties and closed-loop performance objectives into the sensor selection process.

The generalized orthonormal basis system identification, performance criteria selection and Full control sensor placement techniques previously discussed are applied to an experimental flexible structure located at the Dynamics and Control Laboratory of Aerospace Engineering Department at the University of Minnesota. The structure is a four story space truss and was designed to capture the important characteristics of a flexible structure such as lightly damped and closely spaced modes.

The thesis is organized as follows: In Chapter 2 definitions of signals and systems are given and an overview of μ analysis and synthesis and H_∞ control design techniques is presented. The experimental University of Minnesota structure is described in Chapter 3. Dimensions, actuator and sensor types and locations are presented together with the data acquisition system. Chapter 4 presents system identification techniques for flexible structures. It begins by explaining the nonparametric identification technique used in obtaining the experimental transfer functions of the structure from time domain data. A least squares frequency domain curve fitting technique is used to obtain the model of the flexible structure. This model is used to provide the a-priori information to the system identification technique based on generalized orthonormal basis functions. Application of identification with generalized orthonormal basis functions to flexible structures and extension of this technique to generate multi-input/multi-output models constitutes the main part of Chapter 4. In Chapter 5 relations between error and feedback signal selection and performance objectives for vibration attenuation of flexible structures is investigated. In Chapter 6 a sensor placement technique based on full control synthesis is developed. Experimental results of output feedback controllers designed for the sensor locations chosen by this technique is presented. Chapter 7 gives a summary and discussion of the results and suggestions for future work.

Chapter 2

Robust Control Design and Analysis Techniques

The objective of control design is to stabilize the system and improve its performance in the presence of model inaccuracies or uncertainties. It is assumed that the behavior of the system can be represented in terms of a mathematical model and the mismatches between the mathematical model and the true system, the changes in the system parameters due to aging, damage, environmental changes etc. are the sources of uncertainties.

Analysis of a control system consists of quantifying the stability and performance characteristics of the system. In this thesis, H_∞ and μ-synthesis (D-K iteration) techniques are used for designing controllers for the flexible structures and complex and real/complex μ-analysis techniques are used to analyze the controllers. This chapter presents an overview of these techniques. The design method used for optimal placement of sensors is based on Linear Matrix Inequalities (LMI). This technique along with a brief introduction to LMIs is presented in Chapter 6.

2.1 Signals and Systems

In the time domain, finite dimensional linear systems can be represented as sets of linear ordinary differential equations and signals as Lebesgue measurable (for practical purposes, piece-wise continuous) functions of time. Using Laplace transform, both signals and systems can be represented as functions of a complex variable, "s". In this chapter, unless otherwise stated, systems (matrix valued functions of s) will be denoted by upper case letters, such as $G(s), H(s)$ and signals will be denoted by lower case letters, such as in time domain, $x(t), y(t)$ and in frequency domain, $x(s), y(s)$. Signals and systems are classified into spaces based on their properties. Following are the definitions for some of the signal and system spaces related to H_∞ control theory.

Definition 2.1.1 *(***2-norm of a signal***) 2-norm of a signal (the energy of the signal) is*

$$\|x(t)\|_2 = \left(\int_{-\infty}^{\infty} |x(t)|^2 dt\right)^{\frac{1}{2}}$$

Definition 2.1.2 *(***Lebesgue 2-space***) The set of signals for which the 2-norm is finite is the Lebesgue 2-space:*

$$\mathcal{L}_2 = \{x(t) : \|x(t)\|_2 < \infty\}$$

Definition 2.1.3 *(*L_∞ **norm***)* L_∞ *norm of a system is the supremum of the singular value when the transfer function matrix is evaluated on the jw axis.*

$$\|G\|_\infty = \sup_\omega \overline{\sigma}(G(jw))$$

Definition 2.1.4 *(*L_∞ **space***) The space of systems for which the* L_∞ *norm is finite is the* L_∞ *space.*

$$L_\infty = \{G : \|G\|_\infty < \infty\}$$

.

Definition 2.1.5 *(H_∞ **space**) The set of systems analytic on the right half plane with a finite infinity norm is called the H_∞ space.*

2.2 H_∞ Optimal Control

Measuring the performance of a system in terms of the ∞ norm rather than the 2-norm has advantages in dealing with the uncertainties arising in control design [55]. Consider the linear time invariant systems M and Δ. The ∞ norm of these systems satisfy the submultiplicative property:

$$\|M\Delta\|_\infty \leq \|M\|_\infty \|\Delta\|_\infty$$

The small gain theorem ([55, 57]) states that a feedback loop consisting of stable systems is stable if the the loop-gain is less then unity. Submultiplicative property together with the small gain theorem states that a plant M is robustly stable to perturbations Δ entering the system as shown in Figure 2.1 with $\|\Delta\|_\infty \leq \gamma$ if $\|M\|_\infty \leq 1/\gamma$.

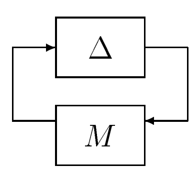

Figure 2.1: Small gain problem

The goal of H_∞ design is is to minimize the ∞ norm of the system M in order to increase the robustness of the system to the uncertainties represented in the Δ block. In H_2 control the uncertainties in signal and system components are modeled as stochastic processes whereas in H_∞ control they are modeled as elements of a bounded set. Following are the descriptions of modeling uncertainties in H_∞ framework:

Parametric Uncertainty Parameters in a state space or transfer function representation of a system are assumed to lie in a set given as

$$p \in \{p_0 + w\delta, \delta \in [-k, k]\}$$

where p_0 is the nominal value of the parameter. δ is allowed to take any value between $-k$ and k and w is the problem dependent scaling factor. It is common practice to scale the parametric uncertainty such that k is 1. This type of uncertainty is suitable in representing uncertain natural frequency and damping levels in flexible structure modes.

Additive and multiplicative uncertainties

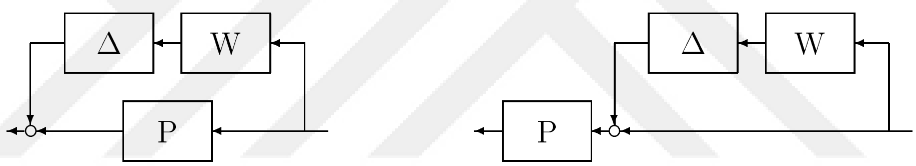

Figure 2.2: a) Additive uncertainty b) Multiplicative uncertainty

The nominal model is assumed to be in the set

$$\{P_0 + \Delta W, ||\Delta|| < 1\}$$

for additive uncertainty and

$$\{P_0(I + \Delta W), ||\Delta|| < 1\}$$

for the multiplicative uncertainty descriptions. In these representations Δ is a variable, norm bounded stable transfer function and W is a fixed stable transfer function compatible with the Δ block.

Coprime factor uncertainty

Perturbing the coprime factors of the model separately allows the introduction of unstable uncertainty. The set of plants is represented by

$$P \in \{(N_0 + \Delta_N)(M_0 + \Delta_M)^{-1}, ||[\Delta_M \;\; \Delta_N]|| \leq \epsilon\}$$

where N_0 and M_0 are the coprime factors of the nominal plant $P_0 = N_o M_0^{-1}$ and Δ_M, Δ_N denote the uncertainty on each factor [56, 18]. Figure 2.3 shows the block diagram representation for right coprime factor uncertainty.

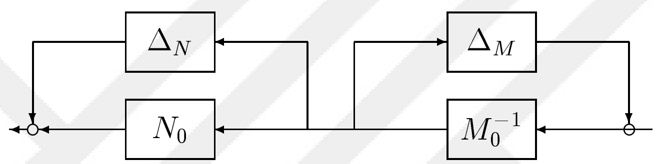

Figure 2.3: Coprime factor uncertainty

In general an uncertain system can be represented in a linear fractional transformation (LFT) form as shown in Figure 2.4. In this figure, G is the nominal model together with uncertainty and performance weights and, for analysis problems, the controller may be absorbed in G. Δ is a block diagonal matrix with different types of uncertainties as the block diagonal elements.

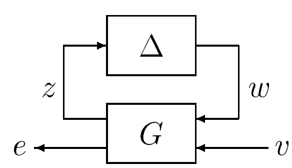

Figure 2.4: Upper Linear Fractional Transformation Structure

The transfer function G can be partitioned as:

$$G = \begin{bmatrix} G_{11}(s) & G_{12}(s) \\ G_{21}(s) & G_{22}(s) \end{bmatrix}; \qquad \begin{bmatrix} z \\ e \end{bmatrix} = G \begin{bmatrix} w \\ v \end{bmatrix}; \qquad w = \Delta z$$

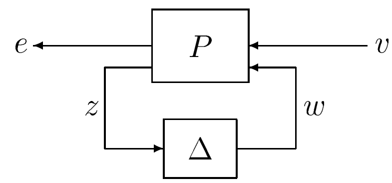

Figure 2.5: Lower Linear Fractional Transformation Structure

Δ block is such that the set of equations is well posed and the vectors e and v are related by

$$e = F_u(G, \Delta)v$$

where

$$F_u(G, \Delta) = G_{22} + G_{21}\Delta(I - G_{11}\Delta)^{-1}G_{12}$$

is called an upper linear fractional transformation of G with Δ. Similarly, the transfer function from inputs to outputs when lower loop is closed with Δ is

$$F_l(G, \Delta) = G_{11} + G_{12}\Delta(I - G_{22}\Delta)^{-1}G_{21}$$

This is called a lower LFT (Figure 2.5).

Following are some definitions and theorems related to H_∞ control problem. Proofs of these theorems are given in [16].

Robust Stability: The controller must stabilize all plants defined by the uncertainty description $F_u(G, \Delta)$.

Theorem 2.2.1 *The LFT $F_u(G, \Delta)$ is stable for all stable $\Delta(s)$ with $\|\Delta\|_\infty \leq 1$ if and only if $\|G_{11}\|_\infty < 1$*

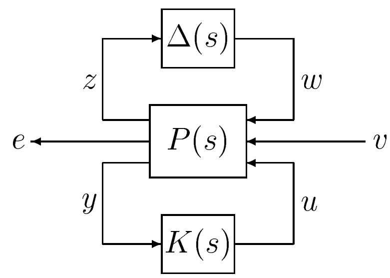

Figure 2.6: General Structure

Nominal Performance: In addition to stability the closed-loop system should satisfy performance requirements.

Theorem 2.2.2 *Nominal performance is achieved if and only if* $\|G_{22}\|_{\infty} < 1$.

Robust Performance: The performance specifications must be satisfied by the closed-loop system for all plants defined by the uncertainty description.

Consider the general framework shown in Figure 2.6. $P(s)$ represents the system interconnection structure, K the controller and Δ the perturbations or uncertainties. v is a vector of exogenous inputs such as reference commands, disturbances and noise. e is a vector of error signals to be kept small, y is a vector of sensor measurements and u is a vector of control signals.

For design purposes the Δ block is eliminated and the input-output map from $[w\ v]^T$ to $[z\ e]^T$ is expressed in LFT form as

$$\begin{bmatrix} z \\ e \end{bmatrix} = F_l(P, K) \begin{bmatrix} w \\ v \end{bmatrix}$$

This structure is shown in Figure 2.7. For the H_∞ optimal control problem, the objective is to find a stabilizing controller K which minimizes $\|F_l(P, K)\|_\infty$.

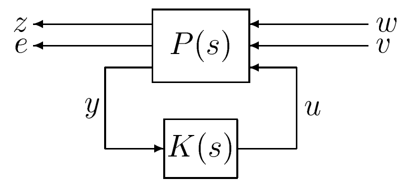

Figure 2.7: Synthesis structure

Initially the H_∞ problem was formulated in an input output framework [54, 55]. The solution techniques were based on Nevanlinna-Pick interpolation or methods based on operator theory [47, 1]. These techniques had difficulties in solving multi-input/multi-output systems. In the following years state space algorithms were developed to solve the H_∞ control problem [16]. These state space techniques are based on solution of two Riccati equations which originate from the separation structure of the controller in the form of full state feedback and optimal state estimation. This structure is similar to the H_2 control problem.

2.3 Structured Singular Value (μ)

The limitation of the H_∞ control design is that the uncertainty structure in the problem is not taken into account. In general, a system is built from components which are themselves uncertain with norm bounded perturbations. This results in the structure of the uncertainty block Δ. The norm bounds given by Theorems 2.2.1 and 2.2.2 are too conservative for realistic problems with structured uncertainty. The structured singular value μ is introduced to reduce this conservatism, see [15, 17, 3].

General framework for μ-analysis is given in Figure 2.4. The Δ block in this representation is defined to have a special structure. $\Delta \in \mathbf{\Delta}$ where $\mathbf{\Delta}$ is a set of block diagonal matrices defined as

$$\mathbf{\Delta} = \Big\{ \Delta = diag \left(\delta_1^R I_{R_1}, \ldots, \delta_m^R I_{R_m}, \delta_1^C I_{C_1}, \ldots, \delta_n^C I_{C_n}, \Delta_1, \ldots, \Delta_p \right) \\ : \delta_i^R \in \mathbf{R}, \delta_i^C \in \mathbf{C}, \Delta_i \in \mathbf{C}^{c_i \times c_i} \Big\}$$

This block structure is general enough to allow for repeated real scalars, repeated complex scalars and full complex blocks.

Definition 2.3.1 *(**Structured Singular Value** μ) For $M \in C^{n\times n}, \mu_\Delta(M)$ is defined*

$$\mu_\Delta(M) = \frac{1}{\min\{\bar{\sigma}(\Delta) : \Delta \in \mathbf{\Delta}, det(I - M\Delta) = 0\}}$$

if no $\Delta \in \mathbf{\Delta}$ makes $(I - M\Delta)$ singular then $\mu_\Delta(M) = 0$

An exact solution for μ does not exist, a solution can be approximated via upper and lower bounds on μ. The method of approximation depends on the structure of the Δ block. If the Δ block does not contain any real elements, the upper and lower bounds for μ can be found by using scaling matrices Q and D. Let

$$\mathbf{Q} = \{Q \in \Delta : Q^* Q = I_n\}$$

$$\mathbf{D} = \Big\{ D = diag \left(D_1^R, \ldots, D_m^R, D_1^C, \ldots, D_n^C, d_1^c I_{c_1}, \ldots, d_p^c I_{c_p} \right) \\ : D_i^R = D_i^{R^*} \in \mathbf{C}^{R_i \times R_i}, D_i^C = D_i^{C^*} \in \underline{i}gCC_iC_i, d_i = d_i^* \in \mathbf{C} \Big\}$$

$\mathbf{Q}$ and $\mathbf{D}$ leave Δ invariant in the sense that if $\Delta \in \mathbf{\Delta}, Q \in \mathbf{Q}$ and $D \in \mathbf{D}$ then $\bar{\sigma}(\Delta Q) = \bar{\sigma}(Q\Delta)$ and $D\Delta D^{-1} = \Delta$

Upper and lower bounds for μ are

$$\sup_{Q \in \mathbf{Q}} \rho(MQ) \leq \mu(M) \leq \inf_{D \in \mathbf{D}} \bar{\sigma}(DMD^{-1}) \tag{2.3.1}$$

The case when Δ contains real elements is more complicated. In order to exploit the real block structure, **G** matrices are needed in addition to **D** scalings.

The set of scalings, **G**, affect only the real parametric uncertainty blocks.

$$\mathbf{G} = \Big\{ G = diag\left(G_1, \dots, G_m, 0_{C_1}, \dots, 0_{C_n}, 0_{c_1}, \dots, 0_{c_p}\right) \\ : G_i = G_i^* \in \mathbf{C}^{R_i \times R_i} \Big\}$$

If there is a $\beta > 0, D \in \mathbf{D}$ and $G \in \mathbf{G}$ such that

$$\overline{\sigma}\left[(I+G^2)^{-\frac{1}{4}}(\frac{1}{\beta}DMD^{-1} - jG)(I+G^2)^{-\frac{1}{4}}\right] \leq 1$$

then

$$\mu_\Delta(M) \leq \beta$$

This β value can be formulated as a Linear Matrix Inequality and solved by convex programming techniques [13, 28, 3].

The structured singular value μ can be used to evaluate the robustness margins for a linear system with structured uncertainty. Consider the following theorem

Theorem 2.3.2 *(***Robust stability***)*

$$F_u(G,\Delta) \;\; \textit{is stable} \;\; \forall \Delta \in \boldsymbol{\Delta} \;\; \textit{iff} \;\; \sup_{w} \;\; \mu(G_{11}(jw)) \leq 1, \;\; 0 \leq w \leq \infty$$

This theorem provides a test for the stability of the system shown in Figure 2.4 for all allowable perturbations. Usually stability is not the only property of a feedback system that must be robust to perturbations. The effect of disturbances on the error signals can increase greatly and performance may degrade significantly when the nominal modal is perturbed. A robust performance test is necessary to indicate the worst case level of performance associated with a given level of perturbations.

The robust performance problem can be formulated as a robust stability problem by associating a fictitious full block of uncertainty, Δ_{perf}, with the performance inputs and outputs. The robust performance problem is equivalent to a robust stability problem but with respect to a different block structure. Consider a new $\underline{\Delta}$ structure defined as

$$\underline{\Delta} = \{ \begin{bmatrix} \Delta & 0 \\ 0 & \Delta_{perf} \end{bmatrix} : \Delta \in \mathbf{\Delta}, \Delta_{perf} \in C^{n_v \times n_e} \}$$

A robust performance test is given by the following theorem.

Theorem 2.3.3 *(***Robust performance***)*

$$F_u(G, \Delta) \ \textit{is stable and} \ \|F_u(G, \Delta)\|_\infty < 1 \ \ \forall \Delta \in \mathbf{\Delta} \ \ \textit{iff} \ \sup_w \ \ \mu_{\underline{\Delta}}(G(jw)) < 1.$$

This means that performance robustness of a closed-loop system can be evaluated by a μ test across all frequencies. The peak value on the μ plot determines the robustness properties.

2.4 μ-Synthesis (D-K Iteration Technique)

This section gives a brief explanation of the D-K iteration technique, a more detailed description can be found in [3, 58]. The μ-synthesis design technique combines the H_∞ control design with μ-analysis. Considering the standard robust performance μ-analysis framework shown in Figure 2.4, the general structure in Figure 2.6 and Theorem 2.3.3, it is desired to find a controller K achieving

$$\inf_{stabilizing \ K} \ \sup_w \ \ \mu_\Delta\{F_l[P(jw), K(jw)]\}$$

This minimization does not have a closed form solution. Upper bound defined for complex μ in Equation 2.3.1 can be used to approximate the solution. Using this fact the problem can be put in the following form.

$$\min_{stabilizing\ K} \{\min_{D_w \in \mathbf{D}} \{\max_{w} \bar{\sigma}[D_w F_l(P,K)(jw) D_w^{-1}]\}\}$$

or equivalently

$$\min_{stabilizing\ K} \{\min_{D_w \in \mathbf{D}} ||D_w F_l(P,K)(jw) D_w^{-1}||_\infty\} \tag{2.4.2}$$

The magnitude D_w across frequency can be approximated by a real, rational stable, minimum phase transfer function $\hat{D}(s)$, then Equation 2.4.2 becomes;

$$\min_{stabilizing\ K} \{\min_{\hat{D}(s) \in \mathbf{D}} ||\hat{D}(s) F_l(P,K)(s) \hat{D}^{-1}(s)||_\infty\}$$

The approach used in solving this problem is to minimize the above expression for either K or $\hat{D}(s)$ while holding the other constant. For fixed D it becomes an H_∞ optimal control problem. For K fixed D can be formulated as a convex optimization problem. This process is applied iteratively until a satisfactory controller is achieved. It should be noted that this D-K iteration technique assumes that the uncertainty is modeled as complex.

Chapter 3

University of Minnesota Experimental Flexible Structure

The system identification, performance criteria selection and sensor placement techniques discussed in this thesis will be tested on an experimental flexible structure in the Dynamics and Control Laboratory of the Aerospace Engineering Department at the University of Minnesota. The structure is a four story space truss and was designed to capture the important characteristics of a flexible structure such as lightly damped and closely spaced modes. The entire structure, constructed of aluminum, is suspended from a mounting structure fixed to the ceiling. The top three stories are each 0.62 m high and the bottom story is 0.47 m high. The width of each bay is 50.8 cm and they are constructed of 0.64 cm thick aluminum plates in the form of equilateral triangles. Two of the plates are solid and two have 43.2 cm equilateral triangles removed from the center. A set of displacement and velocity sensors are collocated with each actuator located along the diagonals of the third bay. Six noncollocated accelerometers are placed at the 3rd and 4th bays and they measure accelerations along the directions parallel to the sides of the triangular plates they are attached to. A detailed picture of the structure is shown in Figure 3.1. The natural frequencies and damping levels of the modes of the structure are discussed in Chapter 4

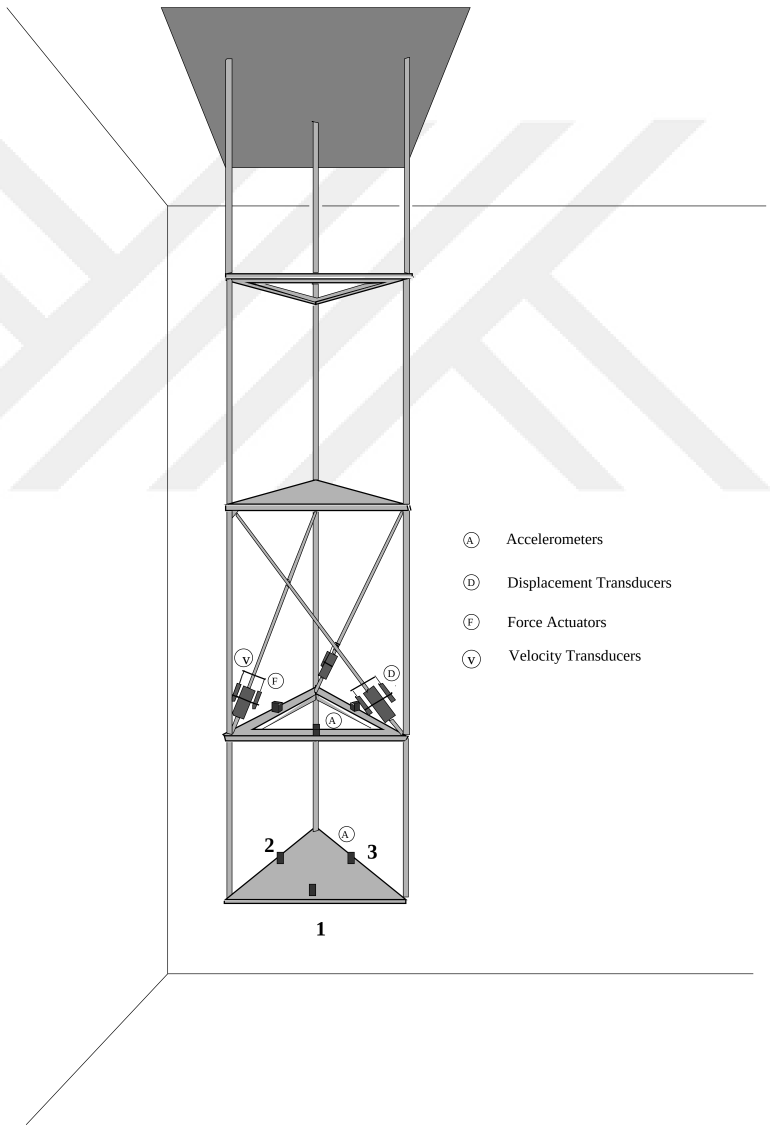

Figure 3.1: Experimental Flexible Structure

3.1 Actuators, Accelerometers, Velocity and Displacement Transducers

The voice coil type actuators are manufactured by Northern Magnetics (ML3-1310-020LB). The input to the actuators are provided by a current amplifier. The actuators can output ± 3 lbs force corresponding to ± 5 volts input to the current amplifier. The bandwidth and stroke length of the actuators are 200Hz and 0.5 inch respectively.

The structure displacements are measured by Trans-Tek 244 LVDTs (linear variable differential transformer). These transducers have a working range of ± 1 inch and a bandwidth of 100 Hz. They require a DC power supply in the 6 to 30 volts range. The displacement measurement are filtered by a 40 Hz, fourth order, low-pass Butterworth filter.

The three velocity transducers are Trans-Tek 114. They provide a voltage output proportional to linear velocity with a sensitivity of 500 millivolts/inch/sec. The bandwidth of these transducers is 120 Hz and the output signals are filtered by a 40 Hz, fourth order, low-pass Butterworth filter.

The accelerometers are of the type ICSensor 3145-002. These accelerometers have a bandwidth of 300 Hz with a sensitivity of 998 millivolts/g. They require a DC power supply in the 6 to 30 volts range.

3.2 Data Acquisition and Real Time Control

The equipment used in acquiring the data and implementing the real time controllers for the experimental flexible structure are a Macintosh IIfx computer, a National Instruments NB-DSP2300 digital signal processing board with a TMS320C30 processor, a National Instruments MIO-16X board and an National Instruments AO-6 analog output board. The computer communicates with the other components via Lab View software package. The MIO-16X board has eight 16 bit differential A/D input channels and two 12 bit D/A channels both with ±10 volt range. The AO-6 board has six 12 bit D/A output channels. The control algorithms are C codes compiled by the DSP board's compiler and loaded on to the DSP board. The Macintosh computer is used for editing and storing the code. Controllers with number of states up to 99 can be implemented on the structure with a 200 Hz sampling rate. Figure 3.2 shows the block diagram of the data acquisition system. An external disturbance is generated by a function generator and added to one of the actuator inputs generated by the computer. The sensor measurements are transmitted to the computer via the A/D board after being filter by the Butterworth filters. The DSP board processes these measurements according to control algorithm and the voltage outputs from the D/A converter is sent to the current amplifier which activates the actuators.

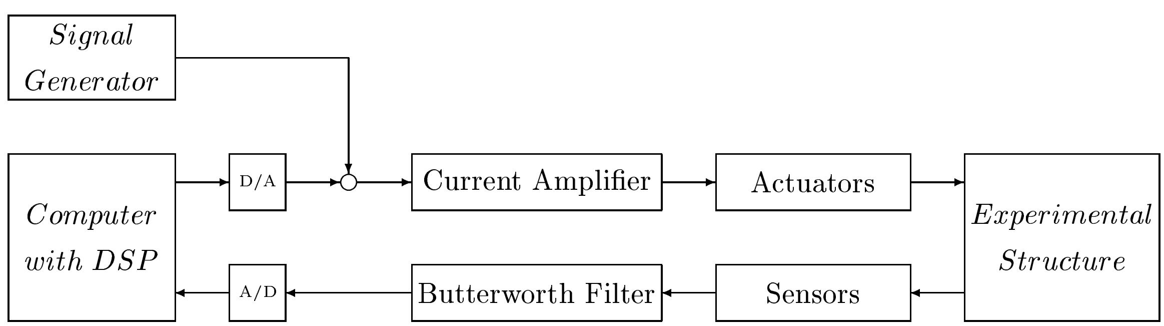

Figure 3.2: Block Diagram of Data Acquisition

Chapter 4

System Identification for Flexible Structures

A dynamical system can be considered as a map (operator) from input signals to output signals. System identification is a method for constructing a mathematical model (an approximate representation) for a dynamical system from input-output data. For complex systems it provides a valuable alternative to modeling from fundamental laws of physics. Experimental results show that the modeling of large flexible structures via finite element method may not be accurate enough for high performance active control design purposes [2].

In this chapter system identification using generalized orthonormal basis functions is developed for flexible structures. This identification technique requires the approximate pole locations of the system being identified as the a-priori information prior to initiating the identification process. It has been shown that generating the basis functions from these approximate pole locations may provide faster convergence for these identification techniques [24]. It is seen that specifying the pole locations at the beginning of the identification process is especially suitable for flexible structures in that a low order multi-input/multi-output (MIMO) model can be realized from individual single-input/single-output (SISO) systems. The approximate pole locations for identification with generalized orthonormal basis function can be obtained either directly from experimental data or from a simpler identification technique. A frequency domain identification technique based on least squares curve fitting is used to find the approximate pole locations for the experimental flexible structure described in Chapter 3.

Both of these identification techniques, least squares curve fitting and identification with generalized orthonormal basis functions, require the frequency response function (Fourier transform of the impulse response function) of the system to be modeled. In Section 4.1 a method of obtaining the system frequency response function, namely, nonparametric identification based on spectral analysis, from input/output time domain data will be explained. Section 4.2 explains the frequency domain identification technique based on least squares curve fitting.

4.1 Nonparametric Identification

The impulse response of a linear, time invariant system characterizes the dynamics of that system. To arrive at parametric representation of a dynamical system, most system identification methods use the Fourier transform of the impulse response function -the frequency response function. Methods of determining these functions from given input/output measurements is called nonparametric identification. Ideally nonparametric identification characterizes the input/output relation of a system without being constrained to a parametrized model set. In practice, however, large number of parameters are used to describe the nonparametric estimate.

In the following section the spectral estimation method of nonparametric identification is explained. Other common methods of nonparametric identification are impulse-response and step-response analysis in time domain and sine-wave testing in frequency domain [32, 37, 11].

First the system to be identified is excited with an input signal $x(t)$ and the output signal $y(t)$ is measured. The input signal should continuously excite the system at the frequency range of interest. A band limited white noise or a sinusoidal signal with continuously changing frequency (chirp) is usually used as input signals [24, 4]. For the University of Minnesota flexible structure, a chirp signal changing from 0.2 Hz to 30 Hz is used. A portion of the time domain representation of this signal is shown in Figure 4.1

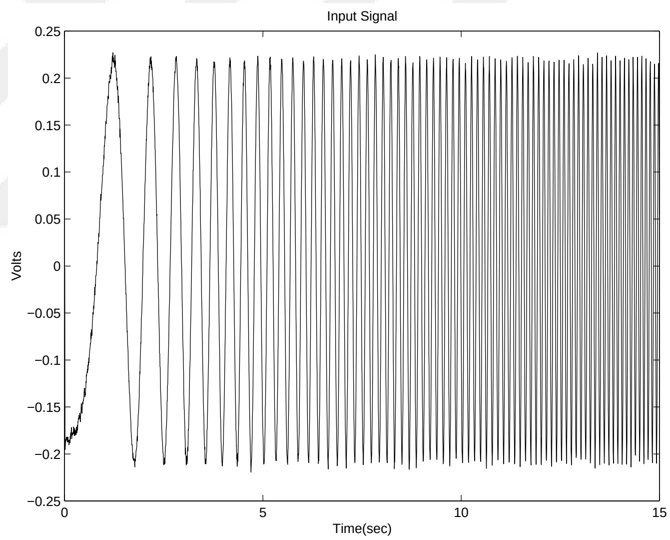

Figure 4.1: Input Signal in Time Domain for Nonparametric Identification

The input/output relation of a linear system is given by the convolution integral

$$y(t) = \int_0^\infty h(\tau)x(t-\tau)d\tau \qquad (4.1.1)$$

where $h(\tau)$ is the impulse response of the system.

The output of an experiment $y(t)$ will have noise due to sensor errors and noise from

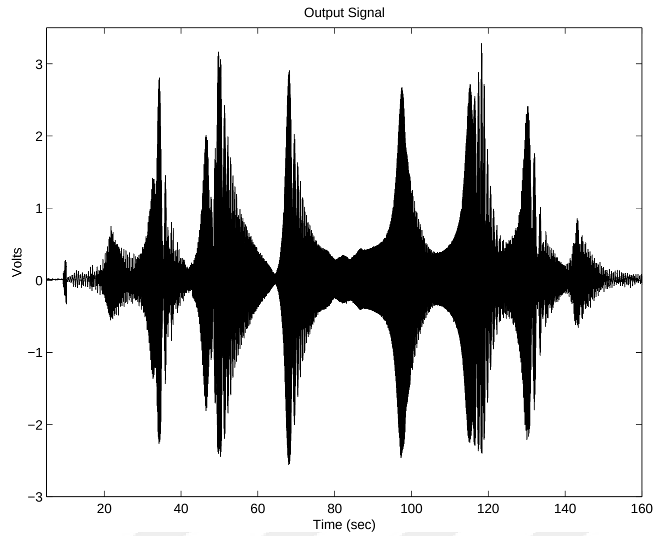

Figure 4.2: Output Signal in Time Domain for Nonparametric Identification

the environment. To reduce the effect of these on the resulting transfer function, correlation technique is used. This computes averages to reduce the effect of noise on the output. In Equation 4.1.1 changing the variables τ to γ, t to $t+\tau$ and multiplying both sides by $x(t)$ leads to

$$x(t)y(t+\tau) = \int_0^\infty h(\gamma)x(t)x(t+\tau-\gamma)d\gamma$$

Calculating the expected values of both sides of the above equation results in the input/output cross-correlation relation

$$R_{xy}(\tau) = \int_0^\infty h(\gamma)R_{xx}(\tau-\gamma)d\gamma \qquad (4.1.2)$$

where

$$R_{xx}(\tau) = \lim_{T\to\infty}\frac{1}{T}\int_0^T x(t)x(t+\tau)dt$$

is the autocorrelation function of $x(t)$ and

$$R_{xy}(\tau) = \lim_{T\to\infty}\frac{1}{T}\int_0^T x(t)y(t+\tau)dt$$

is the cross-correlation function between $x(t)$ and $y(t)$.

The integral in Equation 4.1.2 is a convolution integral. Taking the Fourier transform of this equation gives the relation between power spectral density functions S_{xx}, S_{xy} and the transfer function $H(w)$.

$$S_{xy}(w) = H(w)S_{xx}(w)$$

where

$$S_{xy}(w) = \int_{-\infty}^{\infty} R_{xy}(\tau)e^{-j2\pi w\tau}d\tau$$
$$S_{xx}(w) = \int_{-\infty}^{\infty} R_{xx}(\tau)e^{-j2\pi w\tau}d\tau$$

Plots of power spectral density functions, S_{xx} and S_{xy}, corresponding to the time domain signals in Figures 4.1 and 4.2 are shown in Figures 4.3 and 4.4. The experimental frequency response functions, $H(w)$, for the flexible structure are shown in Figure 4.5.

In most of the recent signal processing software programs the power spectral density functions, S_{xx} and S_{xy} are calculated approximately from the Discrete Fourier Transform of the time domain sequences $x(t)$ and $y(t)$ rather than the correlation functions R_{xx} and R_{xy} due to the numerical advantages of the former technique [31, 24, 35, 45].

4.2 Frequency Domain Least Squares Curve Fitting Technique

An accurate model of the input/output behavior of the system is required for control design. One method to achieve this is by curve fitting a transfer function model

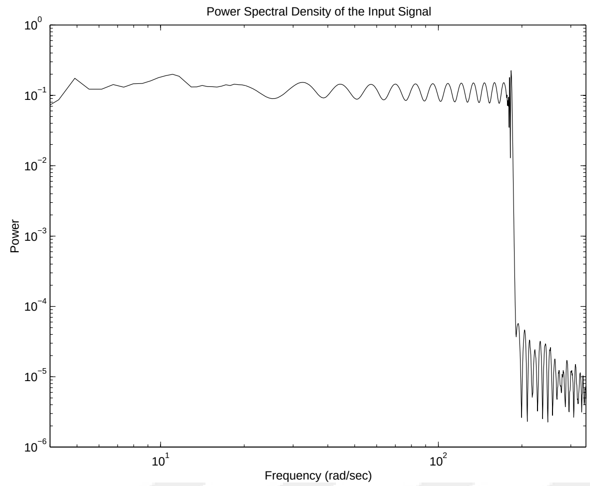

Figure 4.3: Power Spectral Density of the Input Signal

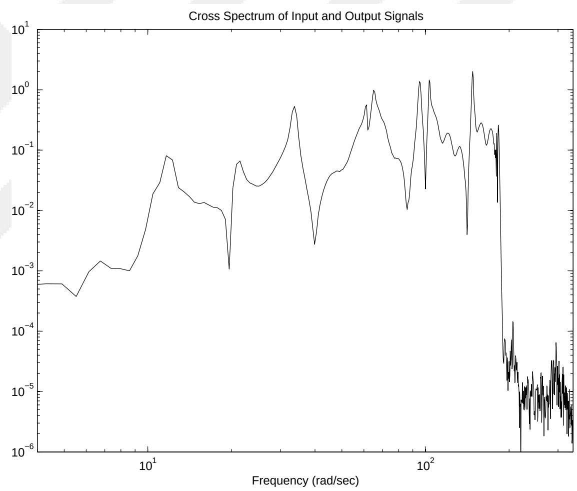

Figure 4.4: Power Spectral Density of the Output Signal

to each non-parametric SISO experimental frequency response function obtained in the previous section (see [10]). These transfer functions are combined to form a multivariable representation of the structure.

Assume that the discrete transfer function representation for each experimental transfer function is given in the form:

$$g(z) = \frac{n(z)}{d(z)} \tag{4.2.3}$$

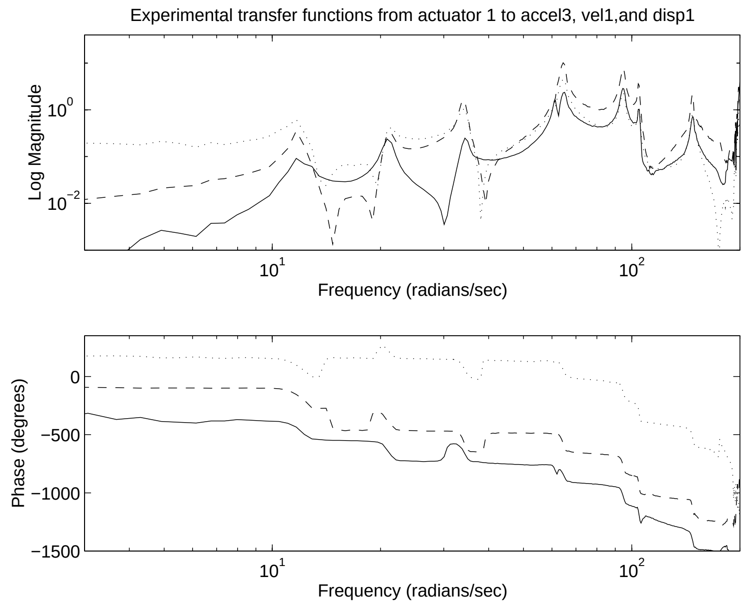

Figure 4.5: Bode plot for the experimental transfer functions

Here $n(z)$ and $d(z)$ are polynomials of degree $\leq$ p with unknown coefficients. Assuming that d is monic, equation 4.2.3 can be written as

$$g(z) = \frac{\sum_{j=0}^{p} n_j z^j}{z^p + \sum_{j=0}^{p-1} d_j z^j}$$

multiplying both sides by the denominator and rearranging gives

$$\sum_{j=0}^{p-1} d_j z^j g(z) - \sum_{j=0}^{p} n_j z^j = -g(z) z^p \tag{4.2.4}$$

Equation 4.2.4 can be put in a compact form by defining the following variables.

$\{z_i\}_{i=1}^{M}$ represents the points on the unit circle obtained by mapping the discrete frequency points ,w_i, of the experimental transfer function, i.e $z_i = e^{j\frac{w_i}{T}}$ where T is the sampling frequency.

$$Z = \begin{bmatrix} \begin{pmatrix} 1 \\ 1 \\ . \\ . \\ 1 \end{pmatrix} & \begin{pmatrix} z_1 \\ z_2 \\ . \\ . \\ z_m \end{pmatrix} & . \quad . & \begin{pmatrix} z_1^p \\ z_2^p \\ . \\ . \\ z_m^p \end{pmatrix} \end{bmatrix}$$

$Z_0 = Z$ with the last column deleted

$D = diag[g(z_1), ..., g(z_M)]$

$\hat{n} = [n_0, ..., n_p]^T$

$\hat{d} = [d_0, ..., d_{p-1}]^T$

$y = [g(z_1)z_1^n, ..., g(z_M)z_M^n]^T$

Hence equation 4.2.4 can be rewritten as

$$(DZ_0 \quad -Z) \begin{pmatrix} \hat{d} \\ \hat{n} \end{pmatrix} = -y \tag{4.2.5}$$

This now is a standard least squares problem. The vectors $\hat{n}$ and $\hat{d}$ can be estimated by solving equation 4.2.5. In the solution an iterative technique is used to remove the high frequency emphasis. The resulting discrete transfer function can be transformed to a continuous system by using bilinear transformation.

This approach is the approach taken in this section to derive a multi-input/multi-output (MIMO) model of the experimental structure. A transfer function model is obtained for each actuator. This results in three 24^{th} order transfer functions from each actuator to all sensors. These three transfer functions are combined and the balanced realization model reduction technique and truncation of the least significant modes results in a 28^{th} order model of the structure [3]. A comparison of this model with the experimental transfer function for the channels from the second actuator to the third accelerometer and to the third displacement sensor is shown in Figure 4.6. Table 1 shows the natural frequencies, damping levels and the mode shapes for the first 12 modes.

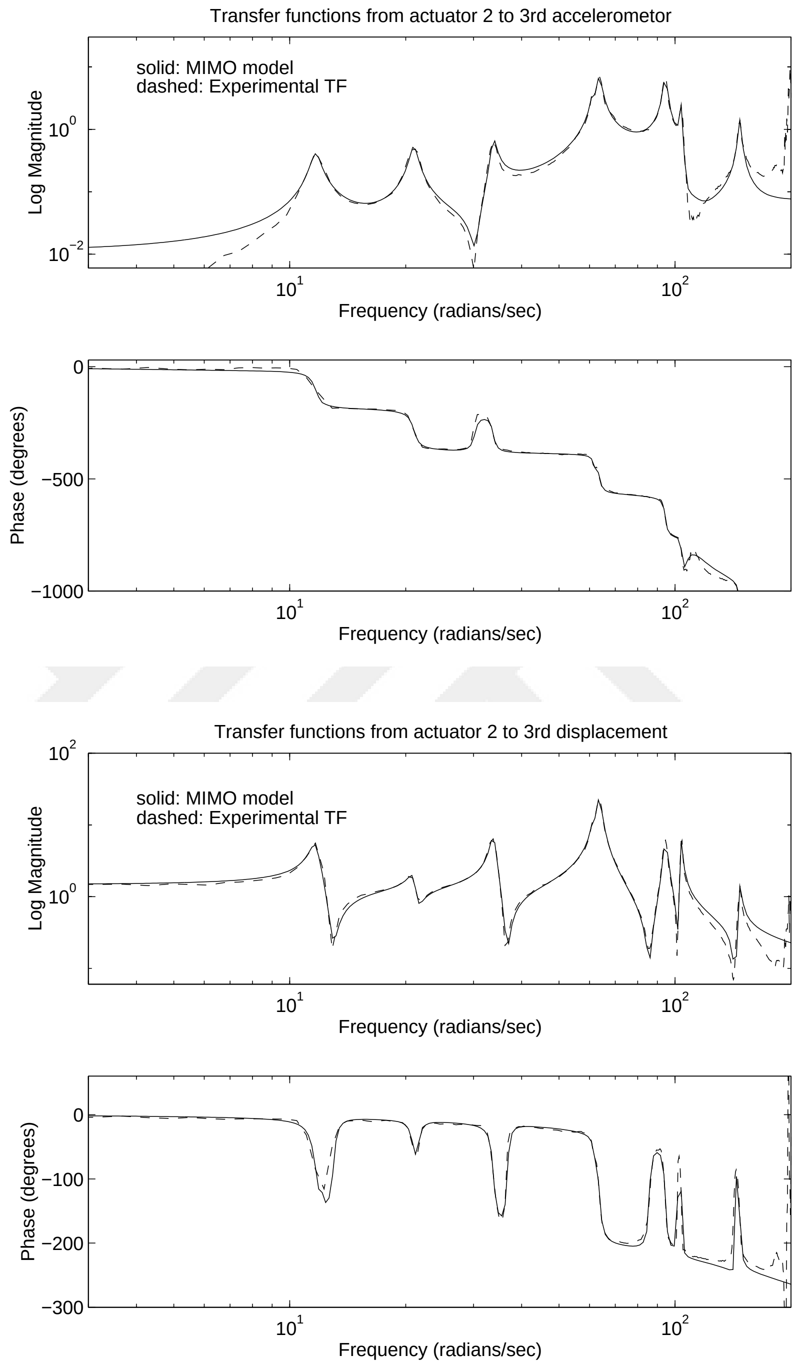

Figure 4.6: Experimental and MIMO Model Transfer Functions

Mode	Natural Frequency (rad/s)	Damping Ratio (%)	Mode Type
1	11.68	2.9	1st X bending
2	11.75	2.7	1st Y bending
3	21.00	2.3	1st torsional
4	33.79	1.6	2nd X bending
5	33.97	1.5	2nd Y bending
6	63.50	1.4	2nd torsional
7	64.21	1.5	3rd X bending
8	64.44	1.1	3rd Y bending
9	94.41	1.0	3rd torsional
10	103.98	0.4	4th X bending
11	104.44	0.5	4th Y bending
12	147.30	0.8	4th torsional

Table 4.1: First Twelve Natural Frequencies of the Flexible Structure

4.3 Identification with Generalized Orthonormal Basis Functions

A model is represented in canonical basis $\{z^{-k}, k = 0, 1, ...\}$ where z^{-1} is a delay operator in classical system identification. If T is the sampling time, a sample u_k at time kT is represented as $u_k z^{-k}$. An alternative to representing a system model in $H_2^{\perp}$ using canonical basis is to represent the system model in terms of the orthonormal basis generated by the a-priori information about the poles of the system. Non-canonical basis have been used successfully in the past for system identification. Two examples of this approach is the use of Laguerre and Kautz systems [51, 50, 44, 52].

Laguerre functions are suitable for constructing orthonormal basis for identification of well-damped systems with one dominating time constant, whereas Kautz functions result in better convergence for lightly damped systems with complex-conjugate poles

[52, 44]. Laguerre and Kautz functions can be obtained as special cases of generalized orthonormal basis functions which are derived from the approximate knowledge about the poles of the system to be identified [22, 36, 49, 19].

Including a-priori knowledge of the system dynamics via the use of orthonormal basis functions into the identification process can have the advantage of reducing the number of parameters to be estimated. Since the resulting model will have the poles specified by the basis functions, only the most significant modes of a system need to be incorporated into the identification procedure. In this thesis it is shown that the ability to choose the significant modes of a model at the beginning of a system identification process is useful in generating a MIMO model from SISO models.

4.3.1 Generating the Orthonormal Basis

A basis in $H_2^{\perp}$ can be constructed by applying Wold decomposition [19, 41]. Let $\{\mu_1, ...\mu_r\}$ be the set of the approximate poles of the system inside the unit disc. Denote by $m(z)$ an all-pass function (finite order Blaschke product)

$$m = \prod_{i=1}^{r} m_i, \quad m_i = e^{j\alpha_i} \frac{1 - \overline{\mu_i} z}{z - \mu_i}, \quad |\mu_i| < 1$$

where α_i is chosen such that $m_i(-1) = -1$.

The following theorem can be used to form a basis in $H_2^{\perp}$ from the poles of a system [19, 12].

Theorem 4.3.1 *Let $H(m) = H_2^{\perp} \ominus m(z) H_2^{\perp}$, then $dim H(m) = r$. Let $\{\varphi_i(z), i = 1, ...r\}$ be a basis for $H(m)$. Then the functions $\{\varphi_i(z) m^l(z), i = 1, ...r; l = 0, 1...\}$ form a complete orthonormal system in $H_2^{\perp}$.*

The orthonormal functions $\varphi_i(z)$ are given by [36, 46]

$$\varphi_i(z) = \frac{\sqrt{1-|\mu_i|^2}}{z-\mu_i} \prod_{j=1}^{i-1} m_j(z) \quad 1 < i < r \tag{4.3.6}$$

Corollary 4.3.2 *A function $f \in H_2^{\perp}$ can be uniquely represented in*

$\{\varphi_i(z)m^l(z), i = 1, ...r; \quad l = 0, 1...\}$ *as*

$$f(z) = \sum_{l=0}^{\infty} \sum_{i=1}^{r} c_{rl+i} \varphi_i(z) m^l(z) \tag{4.3.7}$$

the coefficients of the expansion can be obtained as

$$c_{rl+i} = \langle f(z), \varphi_i(z)m^l(z) \rangle, \qquad i = 1, ...r; \;\; l = 0, 1, 2....$$

where $\langle ., . \rangle$ denotes the usual scalar product in $H_2^{\perp}$.

An expression for the coefficients of the series expansion in equation (4.3.7) can be obtained as follows:

Define $\beta(\vartheta)$ as

$$\beta(\vartheta) = \frac{1}{r} \sum_{i=1}^{r} \beta_i(\vartheta)$$

where β_i are the phase functions of m_i: $m_i(e^{j\vartheta}) = e^{-j\beta_i(\vartheta)}$

Theorem 4.3.3 *Let the model $\hat{f}$ of a system in $H_2^{\perp}$ be parameterized as*

$$\hat{f}(z) = \sum_{l=0}^{n} \sum_{i=1}^{r} \hat{c}_{rl+i} \varphi_i(z) m^l(z),$$

and the measured data set Z be given in the frequency points determined by β^{-1}:

$$Z = \{a_k = f(e^{j\beta^{-1}(s_k)}), s_k = \pi k/N, \;\; k = -N, ..., 0, ..., N-1\}$$

Let N=rM, M∈ $\mathbf{N}$. *The coefficients of the model* $\hat{f}$ *can be expressed as*

$$\hat{c}_{rl+i} = \frac{1}{2M}\sum_{s=-M}^{M-1} F^{v}_{i,s} e^{jls\frac{\pi}{M}} \tag{4.3.8}$$

where

$$F^{v}_{i,s} = \frac{1}{r}\sum_{k=1}^{r} F_{i,s+2(k-1)M}$$

and

$$F_{i,s} = a_s \overline{\varphi}_i(e^{j\beta^{-1}(\frac{s\pi}{rM})}) \frac{r}{\sum_{k=1}^{r} \frac{1-|\mu_k|^2}{|e^{j\beta^{-1}(s\frac{\pi}{rM})}-\mu_k|^2}}$$

Note that the expansion coefficients $\{\hat{c_k}\}$ in equation (4.3.8) are obtained from the inverse discrete Fourier transform of $F^{v}_{i,s}$ and they tend to $\{c_k\}$ as the number of data points tends to infinity.

The method of calculating the coefficients $\{\hat{c_k}\}$ from $F^{v}_{i,s}$ (the virtual frequency domain points) can be illustrated with two examples: Consider the transfer function of a simple first order system given as $sys = \dfrac{2.2}{z-0.9}$. Note that from equation (4.3.6), $\varphi_1(z) = \dfrac{0.44}{z-0.9}$ and $sys = 5\varphi_1$. The normal frequency response and the virtual frequency domain data of this system are shown in Fig. 4.7. Clearly, taking the inverse Fourier transform of virtual frequency domain data, as suggested by equation (4.3.8), gives $c_1 = 5$.

Consider a second example with the system to be identified given as
$sys_2 = \dfrac{2.2}{z-0.9} + 4(\dfrac{0.44}{z-0.9})(\dfrac{1-0.9z}{z-0.9})$.

This system is exactly in the form $sys_2 = c_1\varphi_1 + c_2\varphi_1 m$. Taking the inverse fourier transform of $F^{v}_{i,s}$, shown in Fig. 4.8, gives $c_1 = 5, \;\; c_2 = 4$.

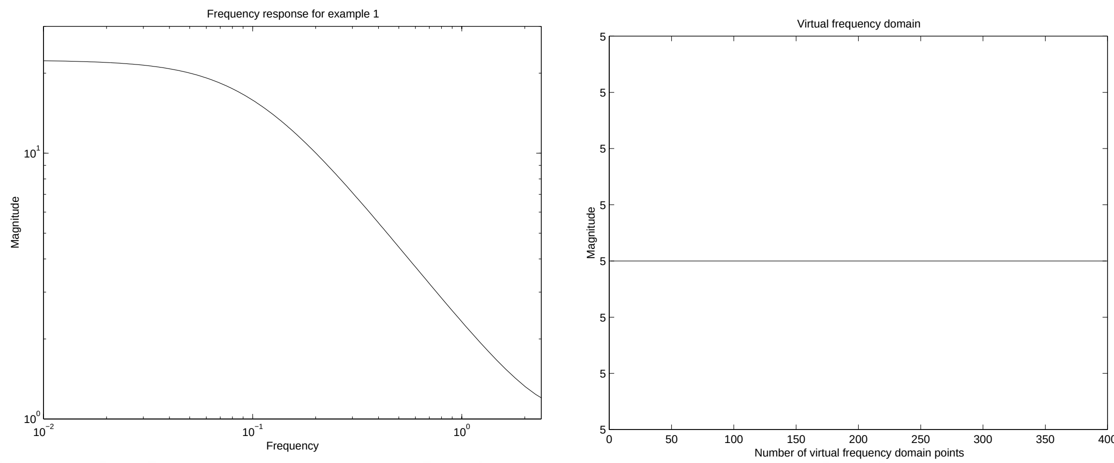

Figure 4.7: Frequency domain and virtual frequency domain data for $\frac{2.2}{z-0.9}$

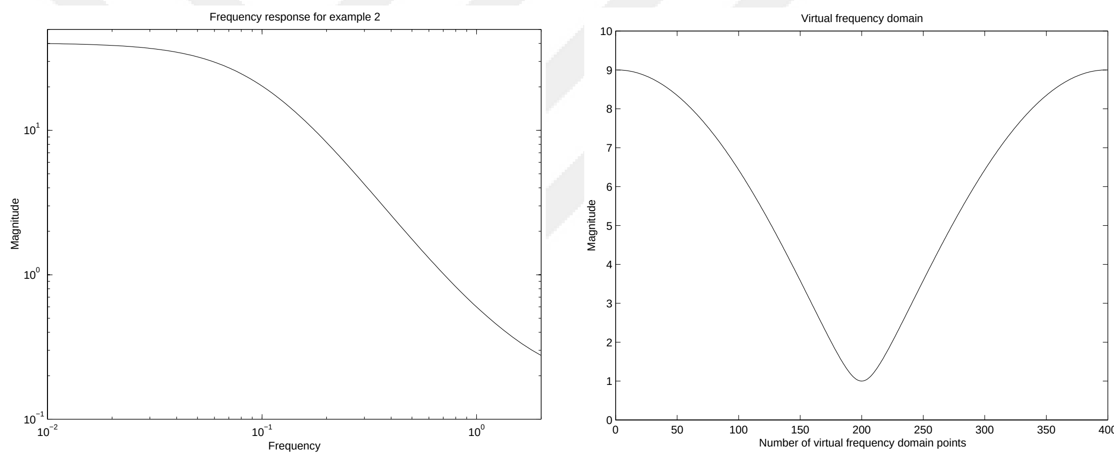

Figure 4.8: Frequency domain and virtual frequency domain data for sys_2

4.3.2 Selection of the approximate pole locations

First step in applying the system-based orthonormal functions in system identification is to obtain the approximate location of the poles of the system that will be identified. For this flexible structure, linear least squares method of identification, explained in Section 4.2, is used to obtain the poles. Models are fitted to the experimental transfer functions from each actuator to the accelerometers with the linear least squares technique. The state order of the models for each input-output channel vary from 16 to 40. The poles resulting from these models are shown in Fig. 4.9 with

$\times, \circ, +$ symbols. Some poles in the least squares identification are for the purpose of adjusting the gain and the phase of the system and do not represent the real poles of the system. These poles show a randomly distributed pattern in Fig. 4.9. Some of the poles from the least squares models, however, are clustered at definite regions of the complex plane. These pole locations are selected as the pole locations of the system model.

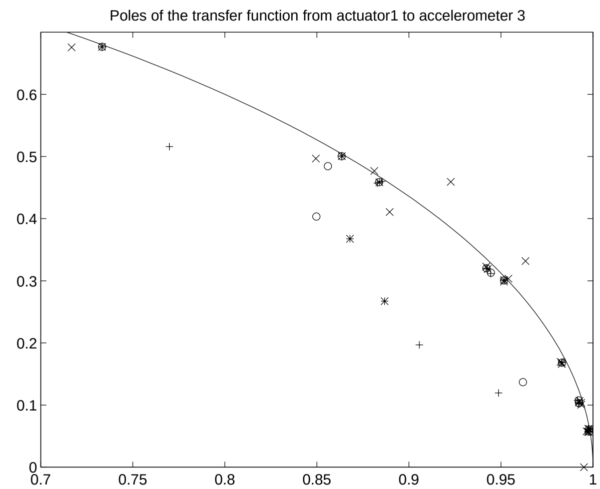

Figure 4.9: Poles of the least square models

4.3.3 Construction of the MIMO State Space Model

The SISO models developed from frequency domain identification using the generalized orthonormal basis are of the form

$$\hat{f}_{ij}(z) = \sum_{l=0}^{M_{ij}} \sum_{i=1}^{r} \hat{c}_{rl+i} \varphi_i(z) m^l(z), \quad ; \; i = 1, ..p, \quad j = 1, ..q \tag{4.3.9}$$

where p and q are the number of inputs and outputs respectively. There are $p \times q$ SISO transfer functions and each of these SISO models are identified individually ie. using a different set of approximate pole locations. The associated MIMO model can be written as

$$\hat{f}(z) = \sum_{l=0}^{M}\sum_{i=1}^{r} \hat{C}_{rl+i}\varphi_i(z)m^l(z), \quad M = max(M_{ij}) \tag{4.3.10}$$

where $\hat{C}_{rl+i}$ are matrices assembled from the coefficients $\hat{c}_{rl+i}$.

Most of the available control analysis and synthesis approaches require models in state space form. One method of realizing the system model given in equation (4.3.10) in state space is based on matrix partial fractional (MPF) representation of MIMO systems. Since the basis functions of $H(m)$ have denominators $d_{p_i}(z) = \Pi_{i=1}^{r}(z - \mu_i)$ the matrix transfer function $\hat{f}(z)$ can be written in MPF form as

$$\hat{f}(z) = \sum_{i=1}^{r} \hat{f}_i(z),$$

$$\hat{f}_i(z) = \frac{R_{K,i}}{(z-\mu_i)^K} + ... + \frac{R_{1,i}}{(z-\mu_i)} \tag{4.3.11}$$

where $K = M + r$

The above form is obtained from the fact that all poles μ_i i=1,...r have multiplicity $K = M + r$ in equation (4.3.10). Using standard results from realization theory, it is known that a minimal realization of $\hat{f}(z)$ can be obtained as a direct sum of minimal state space realizations of $\hat{f}_i(z)$ [20, 23, 25]. This follows from the fact that all the poles of $\hat{f}_i(z)$ are different. The problem now is to construct a minimal realization for all $\hat{f}_i(z)$, $i = 1, 2, ...r$. The elements of this minimal realization are given by the following [34].

Proposition The dimension of a minimal state space realization of $\hat{f}_i(z)$ is given by

$$\mu_i = rank \begin{bmatrix} R_{K,i} & 0 & 0 & . & 0 \\ R_{K-1,i} & R_{K,i} & . & . & . \\ . & . & . & . & . \\ R_{2,i} & . & . & . & . \\ R_{1,i} & R_{2,i} & . & . & R_{K,i} \end{bmatrix} \tag{4.3.12}$$

The proof of the proposition can be obtained by constructing a minimal state space representation and showing that the observability and controllability follows from the above condition.

Proof of Proposition Consider the matrix transfer function $f(z)$ given as

$$f(z) = \sum_{l=1}^{K} \frac{R_l}{(z-\mu)^l} = \frac{1}{z-\mu}(R_1 + \frac{1}{z-\mu}(....\frac{1}{z-\mu}(R_{K-1} + \frac{R_K}{z-\mu})))$$

Define the state variables as

$$\begin{aligned}
&x_1(z) = \tfrac{R_K}{z-\mu}U(z)\\
&x_2(z) = \tfrac{1}{z-\mu}(R_{K-1}U(z) + x_1(z))\\
&x_3(z) = \tfrac{1}{z-\mu}(R_{K-2}U(z) + x_2(z))\\
&.\\
&.
\end{aligned}$$

Applying the inverse Z transform, the state space equations can be written in the form

$$x_{k+1} = \begin{bmatrix} -\mu I_p & 0 & 0 & 0 \\ I_p & -\mu I_p & 0 & 0 \\ & \ddots & \ddots & \\ 0 & 0 & I_p & -\mu I_p \end{bmatrix} x_k + \begin{bmatrix} R_K \\ R_{K-1} \\ \vdots \\ R_1 \end{bmatrix} u_k$$

i.e.

$$x_{k+1} = Ax_k + Bu_k$$

where $A \in R^{Kp \times Kp}, B \in R^{Kp \times q}$, $p = dim(y_t), q = dim(u_t)$, and

$$y_t = \begin{bmatrix} 0 \\ 0 \\ . \\ . \\ I_p \end{bmatrix} x_t$$

It is simple to show that this representation is always observable but not necessarily controllable. The controllability matrix can be written in the form

$$\mathcal{C}(\mathcal{A},\mathcal{B}) = \begin{bmatrix} R_K & 0 & 0 & 0 \\ . & R_K & . & . \\ . & . & . & . \\ R_1 & R_2 & . & R_K \end{bmatrix} \begin{bmatrix} I_p & -\mu I_p & \mu^2 I_p & . \\ 0 & I_p & -2\mu I_p & . \\ . & . & I_p & . \\ 0 & 0 & 0 & I_p \end{bmatrix}$$

where I_p is a $p \times p$ identity matrix. Since the right hand side matrix is of full rank, the rank condition of equation (4.3.12) for the minimal dimension follows.

4.3.4 Application to the U of M Structure

The system identification technique presented in Section 4.3 is applied to the 18 individual channels (3 actuator inputs to 6 accelerometer measurements) of the flexible structure with the pole location determined from the linear least squares fit. The 18 SISO systems are realized as a 58th order state space MIMO model using Matrix Partial Fractional representation technique discussed in Section 3. The order of the MIMO model is reduced to 28 using balanced realization model reduction. A comparison of the 28th order MIMO model, the experimental transfer functions, and the corresponding SISO systems is presented in Figure 4.10 for two channels. From these figures it is seen that there is good agreement between the model and the experimental data and the 28th order model captures the first 12 modes and the 4th order filter characteristics. Hence the assumed pole locations were representative of the actual system. It should also be noted that in this identification technique mismatches in the natural frequencies and damping levels of the model can be corrected by adjusting the assumed pole locations and repeating the identification process with these new pole locations.

The MIMO minimal realization based on Matrix Fractional Expansion is especially suitable for identification with generalized orthonormal basis functions due to the predetermined poles of the system, and since similar poles in different channels are factored together. For large symmetric systems, as is the experimental flexible structure in this research, control over the pole locations results in the minimum number of terms in the matrix partial fraction expansion.

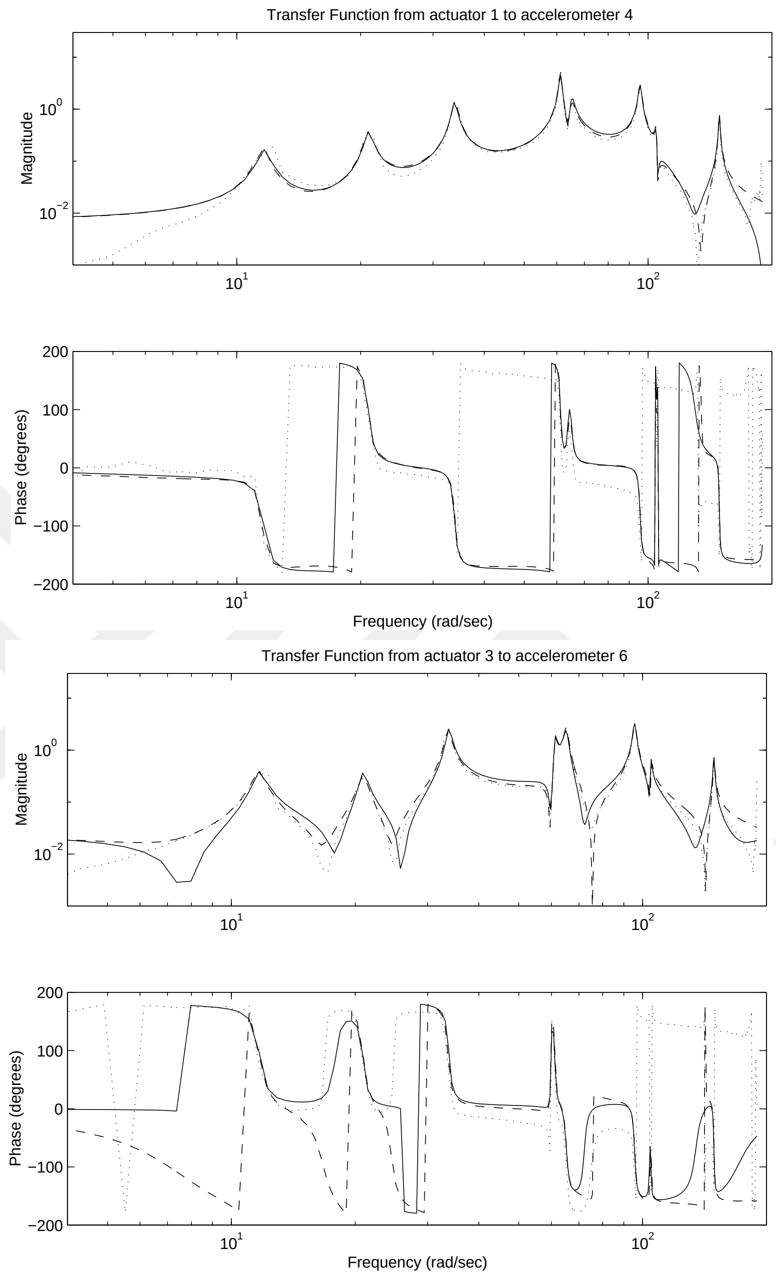

Figure 4.10: MIMO Orthonormal Basis System Model (solid), Experimental Transfer Function (dotted), SISO system (dashed)

4.4 Controller Design

To validate the 28th order MIMO model identified using generalized orthonormal basis functions, a high performance multivariable controller is designed for the experimental flexible structure using the H_∞ control design framework (see [3, 33, 2]). A block diagram formulation of the control problem is shown in Fig. 4.11.

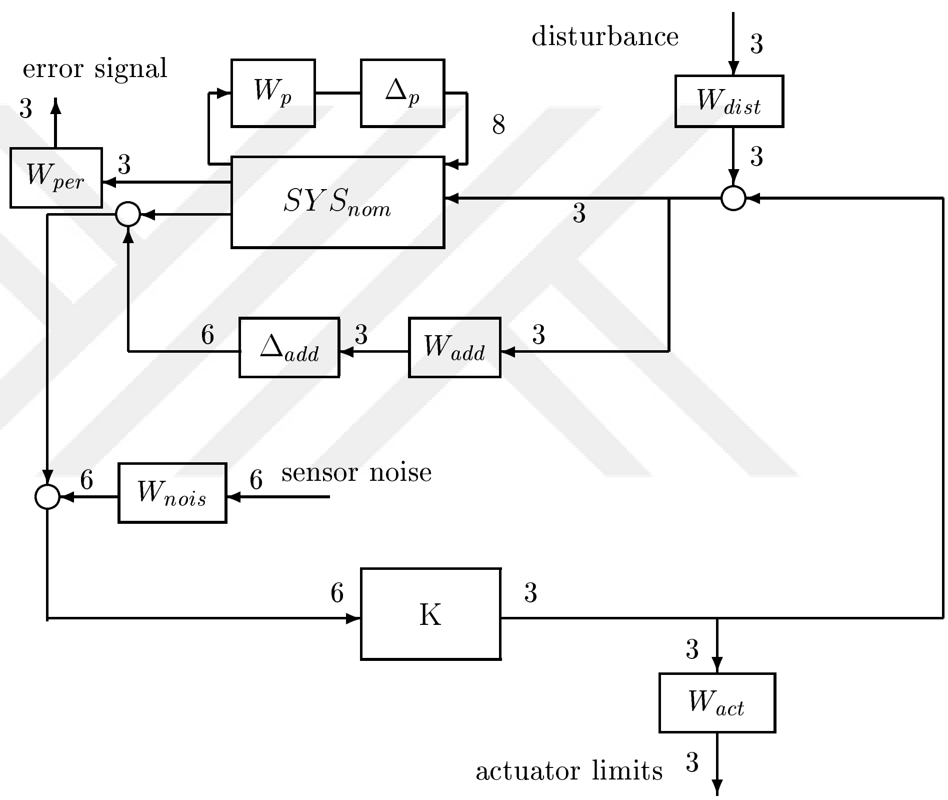

Figure 4.11: Block diagram formulation of the control problem

The performance objective is to attenuate vibration at the bay 4 accelerometer locations due to external disturbances entering at the actuators. (A diagram of the structure and sensor locations is provided in Fig. 3.1). To accomplish this objective, bay 4 acceleration measurements are penalized in the control design, i.e. weighted accelerations are taken as the error signal. Third and fourth bay accelerometers are used as feedback measurements and the three actuators acting along the diagonals of the 3rd bay are used as the control inputs. The frequency range of interest is between 1 Hz and 16 Hz (6.2 and 104 rad/sec) which contains the first ten flexible modes of the flexible structure. Mathematically, the performance objective is defined as minimizing the weighted H_∞ norm of the transfer function from the input disturbance to weighted error outputs. In the H_∞ control problem formulation, the weighting functions are selected so that robust performance is achieved when the structured singular value (μ) of the closed loop system is less than 1.

W_{per} represents a performance weight on the bay 4 acceleration measurements to achieve this objective. The shape of this transfer function and the error signal it is applied to reflect the performance objectives of the controller design process. The maximum singular value of the transfer function matrices from each disturbance input to bay 4 accelerometers are first scaled to one and W_{per} is used to select the desired level of vibration attenuation. For this design W_{per} is a diagonal matrix with w_p as the diagonal elements. w_p is a low pass filter with a DC gain of 4 and cut off frequency at 70 rad/sec. This corresponds to an attenuation ratio of 4:1 in the frequency range of interest.

The input to the voice coil actuators is a voltage from a current amplifier. A one volt command to the current amplifier results in 0.6 lbs of force, with a maximum force of ± 3 lbs. To limit the actuator command signals in the control design process to ± 5 volts ($\pm$3lbs), a value of 1/5 is used to weight each actuator signal. The weight W_{act} is $\frac{1}{5} I_{3\times 3}$.

The weights on the disturbance inputs, W_{dist}, is taken to be the 3×3 identity matrix. This indicates that the input disturbance is on the same order of magnitude as the controller signals. The accelerometer measurement signals have a signal to noise ratio of 100 on all the channels. Based on open-loop experiments, it is expected that the maximum magnitude response of the accelerometers will be ± 1volt. Therefore the sensor noise weight, W_{noise}, in the control interconnection structure, Fig. 4.11, is taken to be 0.01 $I_{6\times 6}$.

An additive uncertainty is included in the problem formulation to account for the unmodeled or neglected high frequency modes, limit the controller bandwidth and modeling errors inside the control bandwidth. This weight is selected to have a magnitude greater than the structural modes above 160 rad/sec. Hence if robust stability of the closed-loop system is achieved for this additive uncertainty weight, the flexible modes of the structure above 160 rad/sec will be gain stabilized. The additive uncertainty weight is given by

$$w_{add} = \frac{18(s^3 + 85s^2 + 7200s + 2.4 \times 10^5)}{s^3 + 1250s^2 + 98600s + 3.5 \times 10^7} \tag{4.4.13}$$

Fig. 4.12 shows the magnitude of w_{add} versus the singular value plot of the transfer functions from actuator 2 to all accelerometers. In the control problem formulation shown in Fig. 4.11, the additive uncertainty W_{add} is a 3×3 diagonal matrix with each diagonal entry as w_{add}.

The pole locations used to derive the MIMO structural model do not exactly correspond to the natural frequencies and damping levels of the structure. (see Figs. 4.3.4 and 4.10). These errors or variations in the first 10 modes are accounted for by introducing parametric uncertainty in the state space coefficients. It is not important to include parametric uncertainty in the other modes since they are to be gain stabilized based on the additive uncertainty weight selected.

Parametric uncertainty is modeled as complex variations in the control design process. Since this may introduce conservatism in the control design, it is important to carefully select which state space entries are to be perturbed. It turns out that

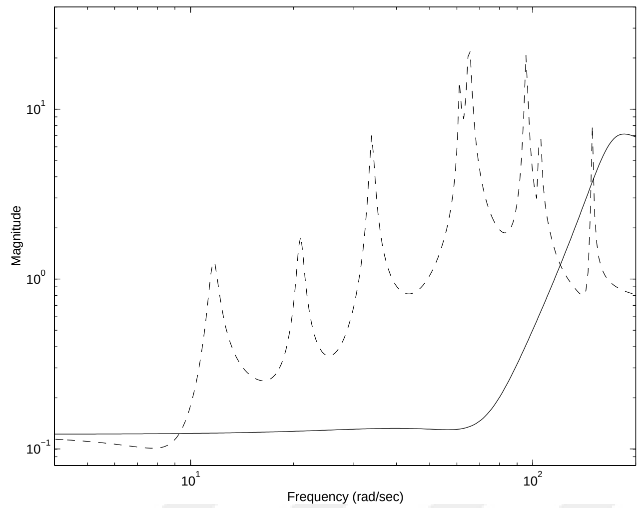

Figure 4.12: Magnitude plot for W_{add}. Experimental transfer function (dashed) W_{add} (solid)

complex perturbations in the damping levels lead to variations in the damping levels and structural natural frequencies in the system model [6, 53]. In this problem, the **A** matrix of the state space realization of the experimental structure is transformed to bidiagonal form and only the first element of each 2×2 natural frequency block is perturbed. This corresponds to complex uncertainty in the damping values of each mode. A complex perturbation of the damping values results in a small change in the natural frequency and a significant change in the damping level of that mode. There is a variation of 0.2% in natural frequency and 15% in damping level of the first mode when the first element of the 2×2 submatrix corresponding to this mode is perturbed by 15%. W_p in Fig. 4.11 is an 10×10 diagonal matrix with 0.05 as the diagonal elements which represents the perturbation on the first elements of the 2×2 bidiagonal modal matrices. This weight corresponds approximately to 15% uncertainty in the damping values of the first 10 modes.

The resulting 6 input, 3 output H_∞ controller has 40 states. Fig. 4.13 shows a singular value plot of the loop transfer function. The controller expends most of its effort in the mid frequency range, the region where the peaks of the loop transfer function singular value plot are above 1, to achieve the desired performance objectives and rolls of around 90 rad/sec. These results are consistent with the shapes of the additive uncertainty and performance weights. The robust stability, nominal performance and robust performance plots for the controller are shown in Fig. 4.14. A maximum value of 0.4 on the robust stability plot indicates that stability is guaranteed for the set of systems described by the uncertainty model. A maximum μ value of 1.2 indicates that a worst case performance level of 1/1.2 is achieved for all the plants with in the uncertainty set. A comparison of solid and dotted lines in Fig. 4.14 shows that there is almost no difference between complex and real/complex μ values. This is due to small parametric uncertainty in the low frequency modes of the model. The system has the modes with the largest amplitude around 80 rad/sec and performance objective dominates at that frequency (robust performance = 1.2 and nominal performance = 1.1). The low value of the robust stability plot at high frequency range shows that the unmodeled dynamics are not the driving factor in the design.

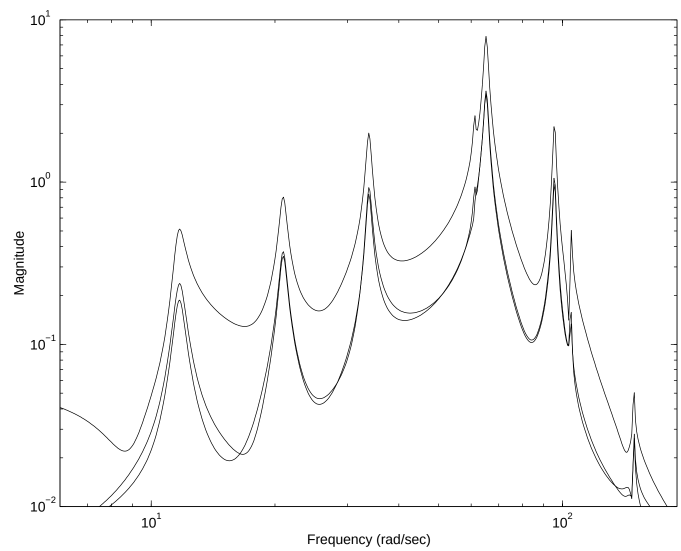

Figure 4.13: Singular value plot of the system loop gain

The controller is implemented on the structure and the responses to a sine-sweep

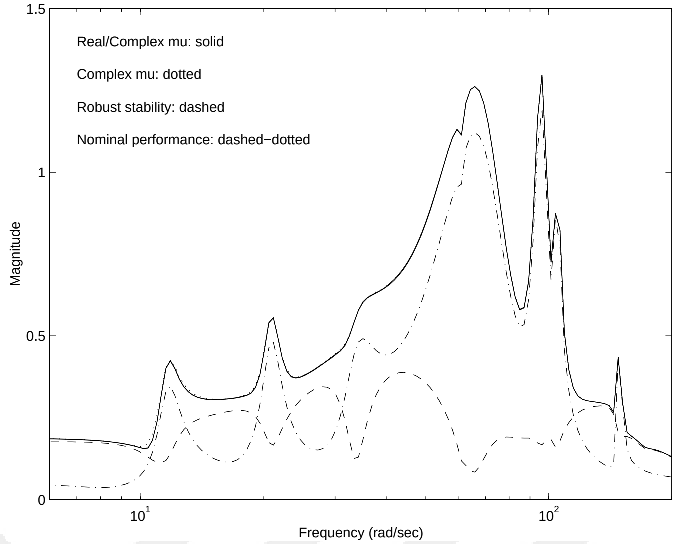

Figure 4.14: μ plot for the closed-loop system corresponding to the interconnection diagram in Fig. 4.11

disturbance through actuator 2 are shown in Figures. 4.15 and 4.16. Experimental results show that an attenuation ratio of approximately 3.5:1 is achieved on channels 1 and 2. This is very close to the desired performance ratio of 4:1. This shows that the real plant is in the set of plants defined by the nominal identified model and the additive and parametric uncertainties.

The simulation results are shown in Figs. 4.15 and 4.16. The amount of attenuation on the simulation results are in agreement with the experimental results. The low frequency peaks of the transfer function in the simulation data are not attenuated as well as the experimental transfer function data. This may be due to smaller damping values for those modes in the identified model than the real system.

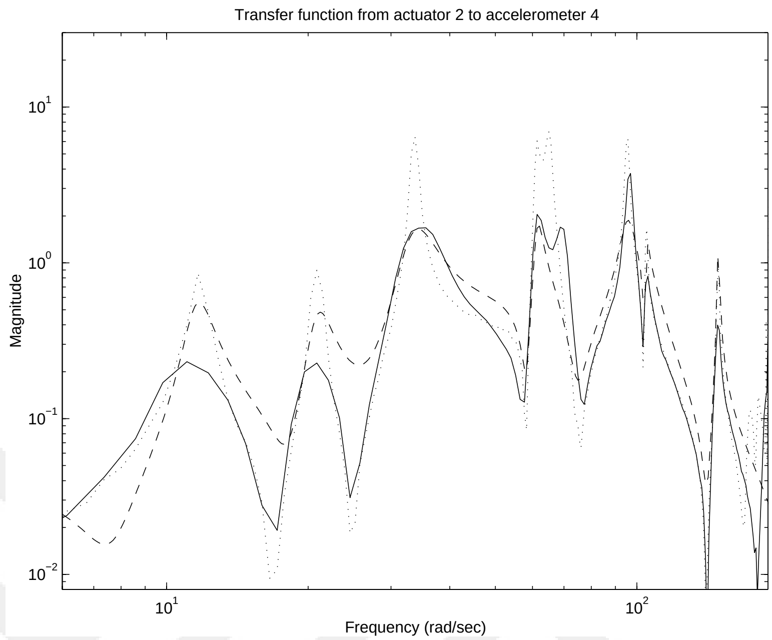

Figure 4.15: Experimental Transfer Functions: closed-loop (solid), open-loop (dotted), closed-loop simulation of the nominal plant (dashed)

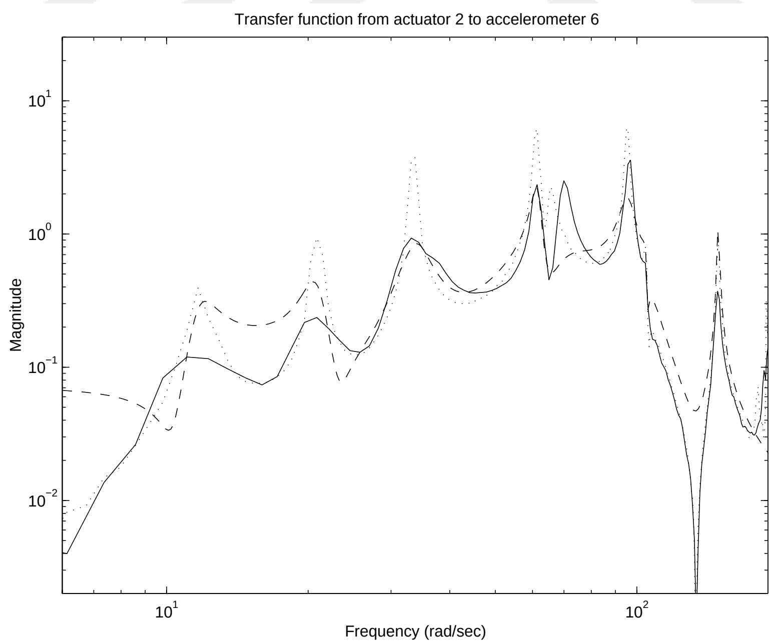

Figure 4.16: Experimental Transfer Functions: closed-loop (solid), open-loop (dotted), closed-loop simulation of the nominal plant (dashed)

Chapter 5

Performance Criteria and Feedback Signal Selection

An interesting area to investigate for active vibration attenuation in flexible structures is the selection of error signals and performance weights that directly reflects the performance objectives. This issue is investigated by designing eight vibration attenuation controllers using μ-synthesis technique in this chapter. Six of these controllers use collocated displacement and noncollocated acceleration feedback, one uses collocated velocity feedback and one uses only noncollocated acceleration feedback. The level of uncertainty is held constant among the controllers using the same feedback information. Performance objectives are related to velocity, acceleration and displacement signals that are penalized in turn at different locations. The results of this investigation show the direct relationship between the weighted error signals and performance.

5.1 Control Problem Formulation and Objectives

Structured Singular Value (μ) synthesis technique is used to design controllers for the flexible structure. For a detailed explanation of this technique see reference [3].

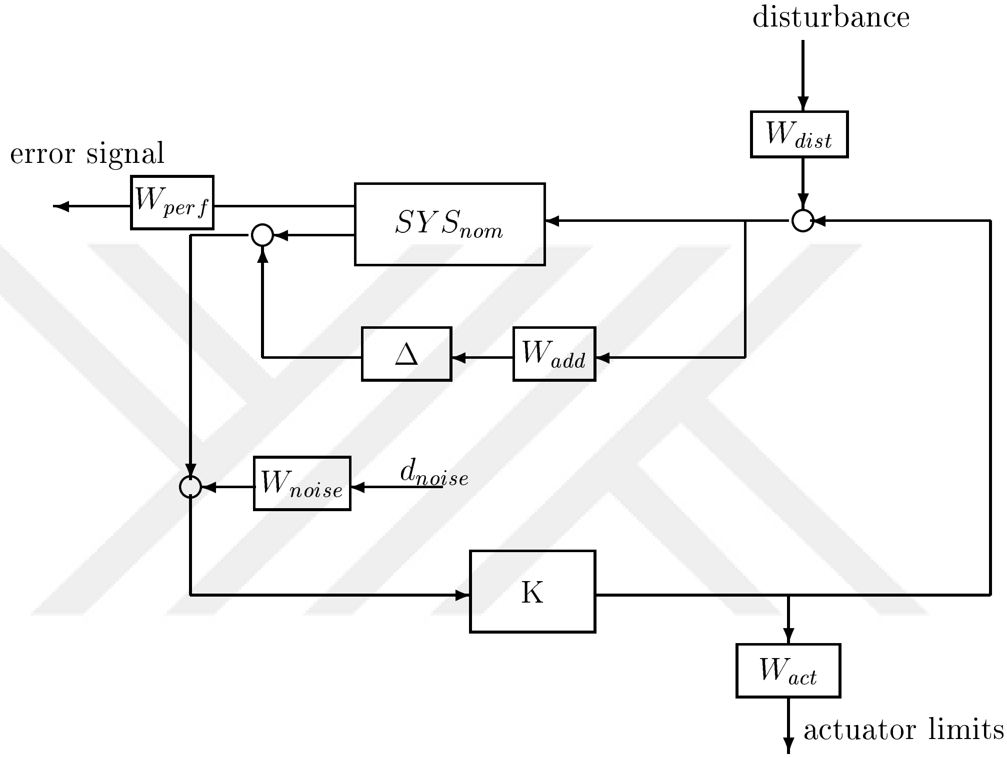

Figure 5.1: Block diagram formulation of the control problem

A block diagram formulation of the control problem is shown in Figure 5.1. SYS_{nom} represents the identified nominal model of the structure. For velocity feedback case this model has three inputs and three outputs and for acceleration/displacement feedback the model has three inputs and six outputs. These models are obtained by the frequency domain least squares curve fitting technique discussed in Section 4.2.

The weight W_{dist} is selected as 1 for each input channel. The noise on the measurement channels are represented by d_{noise}. W_{noise} is a diagonal matrix with diagonal elements equal to 0.01. This represents a signal to noise ratio of 100 on all the

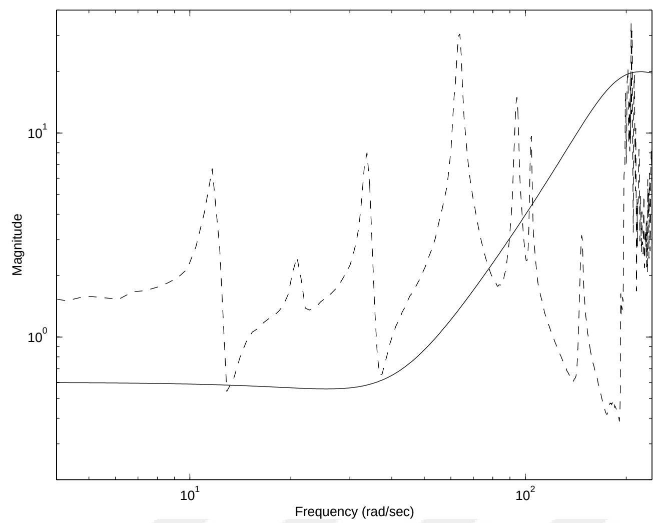

Figure 5.2: Magnitude plot for the additive uncertainty W_{add} (solid) and singular value plot for the experimental transfer function from actuator 2 to all the sensors (dashed)

channels.

W_{act} penalizes the actuator action and is selected to be a diagonal matrix with 0.2 as the diagonal elements. This scales the output of W_{act} to one when the actuator force is ± 3 lbs (see Section 4.4).

Unmodeled dynamics of the structure are accounted for in the control design process via an additive uncertainty model, W_{add}, around the nominal model. The unmodeled dynamics represent high frequency modes outside the desired control bandwidth that may cause instability in the closed-loop system if unaccounted for in the design model. The magnitude of the additive uncertainty weight is selected to cover the transfer function response of these modes. The magnitude plot of W_{add} for displacement/acceleration feedback cases and the singular value plot of the transfer function from actuator 2 to all the sensors is shown in Figure 5.2. The input signal excites the structure up to 190 rad/sec, hence the noisy part of the transfer function above 190 rad/sec in Figure 5.2 does not represent the true dynamics of the structure. In this research W_{add} is held fixed for the designs that use the same feedback information in order to be able to see the effects of performance weight selection on the results. The additive uncertainty weight for displacement/acceleration case is given by

$$W_{add} = \frac{13(s^2 + 45s + 1760)}{s^2 + 1290s + 37500}$$

For velocity feedback case, W_{add} is scaled by 1.25 and for the acceleration feedback case

$$W_{add} = \frac{24(s^3 + 170^2 s + 14300s + 7.62 \times 10^5)}{s^3 + 387s^2 + 46000s + 6.6 \times 10^6}$$

W_{perf} is the transfer function that represents the performance weight. The shape of this transfer function and the error signal it is applied to reflects the performance objectives of the controller design process. This relation will be investigated in detail in the following section.

5.2 Experimental Results

Eight controllers are designed for the flexible structure. Table 5.1 shows the outputs being penalized (error signal), feedback information being used and the location of the error signal for each design. In each design the performance objective is to minimize the maximum transfer function frequency response between the input disturbances and the weighted error signals. The frequency range of interest is between 1 Hz and 16 Hz which contains first nine flexible modes of the flexible structure. The performance weight, W_{perf}, is chosen as a constant value for the frequency range of interest for all the designs in order to make the comparison between the cases easier and more fair, although frequency dependent weights would provide better results in most cases.

	Feedback	Error signal type	Error signal location
case 1	acceleration/displacement	displacement	actuators
case 2	acceleration/displacement	displacement	acceleration sensors
case 3	acceleration/displacement	acceleration	acceleration sensors
case 4	acceleration/displacement	velocity	acceleration sensors
case 5	acceleration/displacement	velocity	actuators
case 6	acceleration/displacement	acceleration	actuators
case 7	velocity	velocity	actuators
case 8	acceleration	acceleration	accelerometer sensors

Table 5.1: Feedback and Error Signals

The disturbance to error signal transfer functions are first scaled to one and W_{perf} is used to determine the amount of attenuation of the frequency response peaks.

A description of each case follows and experimental results are presented in Figures 5.3 - 5.10. In each figure the frequency response of the transfer functions from actuator 2 to accelerometer 3 and displacement sensor 3 are given. The other channels have very similar characteristics to the ones displayed.

Case 1: Displacement error is penalized with a constant weight at actuator locations. From Figure 5.3 it is seen that the controller performs very well in minimizing the displacement error. The peaks are approximately at the same level. This exactly is the goal being posed by a constant performance weight on the displacement channels. Considering the acceleration signals however, the controller has a poor performance. Only the first bending and second torsional modes are attenuated. If the performance objective was the attenuation of vibration in the entire structure, penalizing displacement signals at actuator locations with a constant weight would not be a good choice.

Case 2: Penalizing displacement signals at accelerometer locations which is a noncollocated performance objective improves the attenuation of structural vibration at the third bay. From Figure 5.4 it can be seen that the first and second bending modes are significantly attenuated. It is interesting to note that Controller 2 does almost as good as Controller 1 in attenuating the displacement signals at actuator locations. Overall, Controller 2 performs better in attenuating the vibrations at bay 3 than Controller 1.

Case 3: Controller 3 significantly attenuates the structural vibrations at the accelerometer locations when acceleration signals at accelerometer sensor locations are used as the performance objective. This also is a noncollocated performance objective. Displacement signals at actuator locations are also attenuated. The main difference between Controller 3 and Controller 2 is that Controller 3 attenuates vibrations in the mid frequency range, 30-100 rad/sec, better than Controller 2 although Controller 2 attenuates low frequency vibrations, first bending and torsional modes, better. This is expected since an approximate double integrator is used in design 2 to obtain the displacement signals at accelerometer locations and this emphasizes the low frequency modes more.

Case 4: Selecting the performance objective of minimizing velocity at the accelerometer locations, a noncollocated criteria, results in a controller very similar to Case 2. The low frequency modes are not as significantly attenuated as with Controller 2, although better attenuated than in Controller 3. This again is due to the integrator being used to obtain velocity signals from acceleration measurements. Often the overall performance objective is not just to attenuate acceleration velocity or displacement, therefore a frequency dependent weight would be used to capture the desired performance objective.

Case 5: A similar performance goal is posed for case 5 as case 4. In this case velocity signals are penalized at displacement sensor locations, a collocated performance objective, again with a constant performance weight. From Figure 5.7 it can be seen that the controller performs very well on the displacement channel, all the peaks are at the same level. The acceleration signals are not attenuated as well. This is the main difference between case 4 and 5. This result should also be compared with the first case. The only difference between these cases is the differentiator that creates the velocity signal in case 5. Due to the differentiator action the higher frequency modes are emphasized more and attenuated better in case 5.

Case 6: Controller 6 is designed to minimize the acceleration response at the displacement sensor locations. As can be seen from Figure 5.8, this controller performs very well at the high frequency, 40-120 rad/sec, structural modes at displacement sensor locations. Unfortunately the performance of the controller at accelerometer locations is not as good. Also low frequency modes of the structure are poorly attenuated. This type of controller may be of interest in vibration isolation applications.

Case 7: Controller 7 is designed using velocity sensors collocated with the actuators to attenuate velocity signals at the sensor locations. This is not exactly collocated velocity feedback since cross coupling between the actuators and the sensors is allowed. Overall this controller performs poorly when compared with the previous designs. The main objective of this design is to increase the damping levels of the structural modes, therefore the controller may improve the damping but not the overall magnitude of the response. The results of this design are often not what is desired based on the performance objectives.

Case 8: In case 8 only acceleration feedback is used and a performance weight that approximates a double integrator in the frequency range of interest is applied to the acceleration signals at accelerometer locations. Comparing the results shown in Figure 5.10 with that of case 2 and 3 it is seen that the vibrations in the third bay can be attenuated by using noncollocated acceleration feedback alone. It is an important observation since accelerometers are accurate and can be placed at the desired locations on the structure easily.

5.3 Summary

This chapter focused on the selection of error signals and performance weights for active vibration attenuation in flexible structures. It is shown that the controllers may succeed in achieving what is being asked for by the design criteria but this may not be the overall desired result. As seen in μ-synthesis design the choice of performance weightings and the signals being penalized play an extremely important role and they must be selected based on the performance objectives.

The type of attenuation desired (acceleration, velocity, displacement at collocated and noncollocated locations) and the frequency range of interest are factors that dictate the choice of penalty weights and error signals as well as sensor locations. In the above cases penalizing signals measured at accelerometer locations gave good results. This has the advantage that acceleration measurements are accurate and sensors can be placed anywhere on the structure easily. This flexibility leads to the problem of selecting optimal sensor locations for flexible structures which will be considered in the next chapter.

Collocated velocity feedback did not provide a good level of attenuation at the sensor locations when compared with the other designs. This type of feedback is often used in increasing the damping of the modes but may be a poor choice for attenuating the vibrations at locations other than at the actuators on the structure.

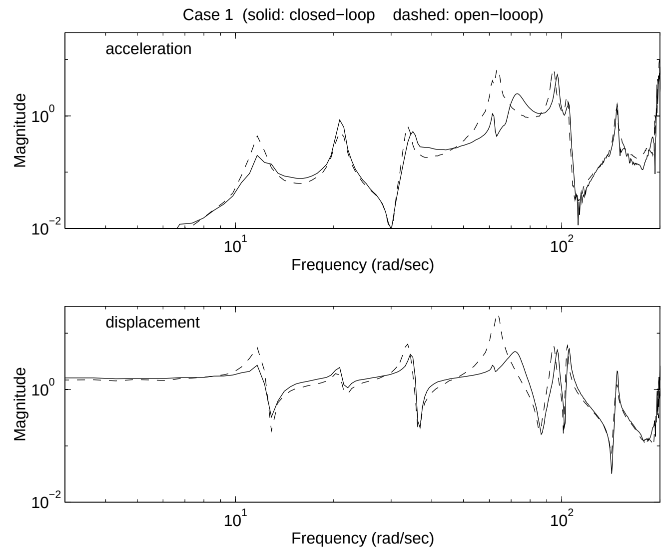

Figure 5.3: Case 1: Frequency response of the transfer functions from actuator 2 to accelerometer 3 and displacement sensor 3. Displacement is penalized at actuator locations.

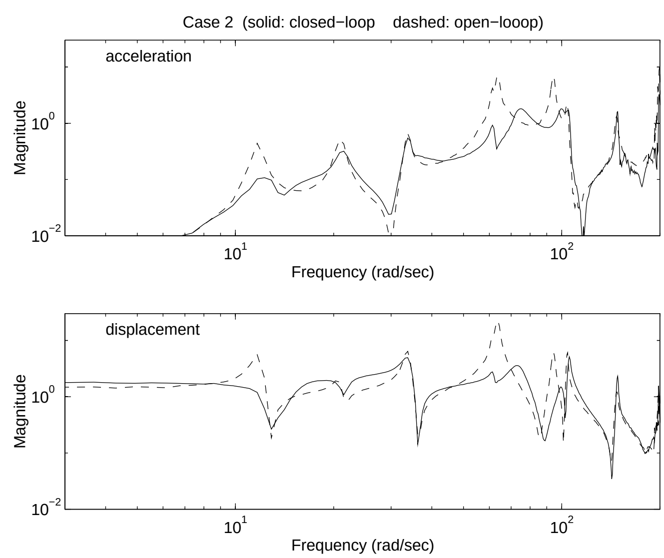

Figure 5.4: Case 2: Frequency response of the transfer functions from actuator 2 to accelerometer 3 and displacement sensor 3. Displacement is penalized at accelerometer locations.

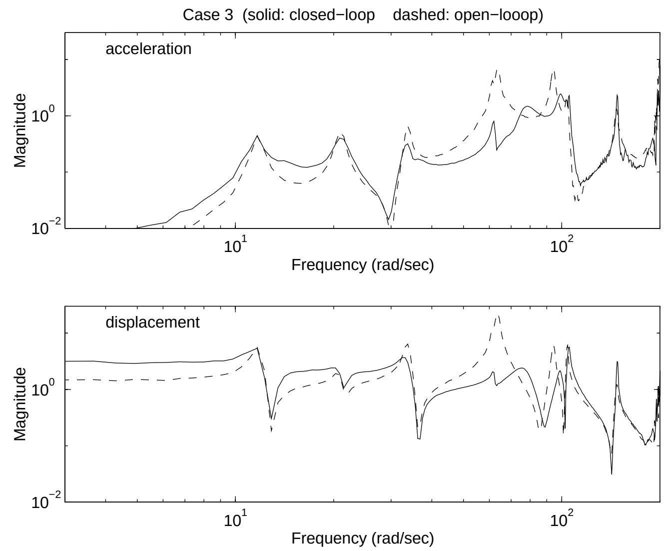

Figure 5.5: Case 3. Frequency response of the transfer functions from actuator 2 to accelerometer 3 and displacement sensor 3. Acceleration is penalized at accelerometer locations.

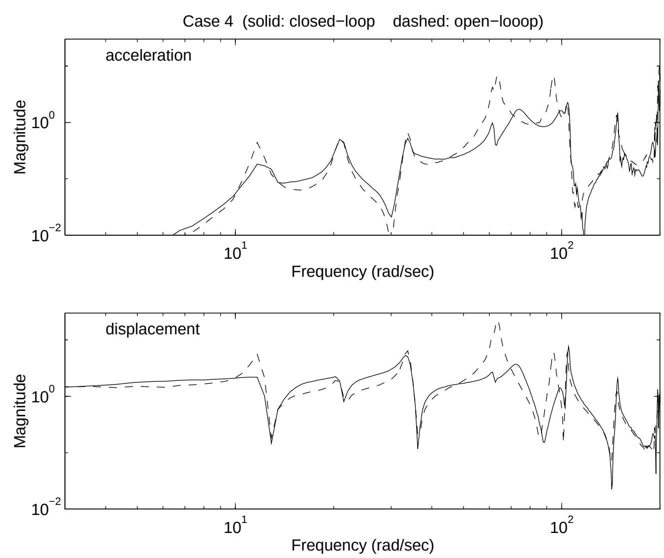

Figure 5.6: Case 4. Frequency response of the transfer functions from actuator 2 to accelerometer 3 and displacement sensor 3. Velocity is penalized at accelerometer locations.

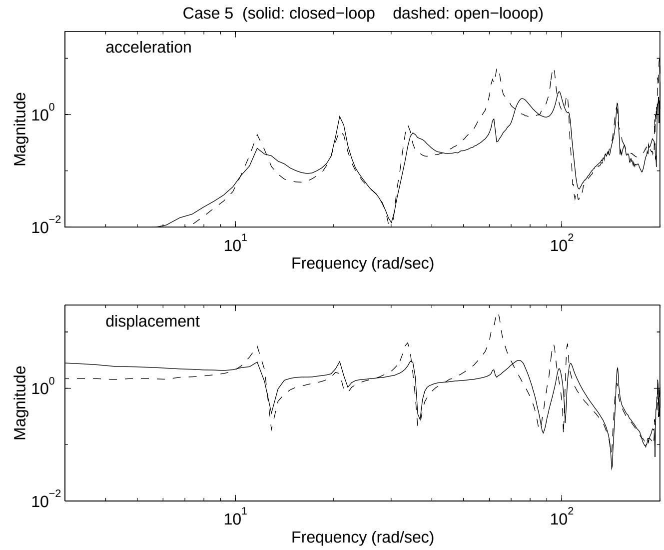

Figure 5.7: Case 5. Frequency response of the transfer functions from actuator 2 to accelerometer 3 and displacement sensor 3. Velocity is penalized at actuator locations.

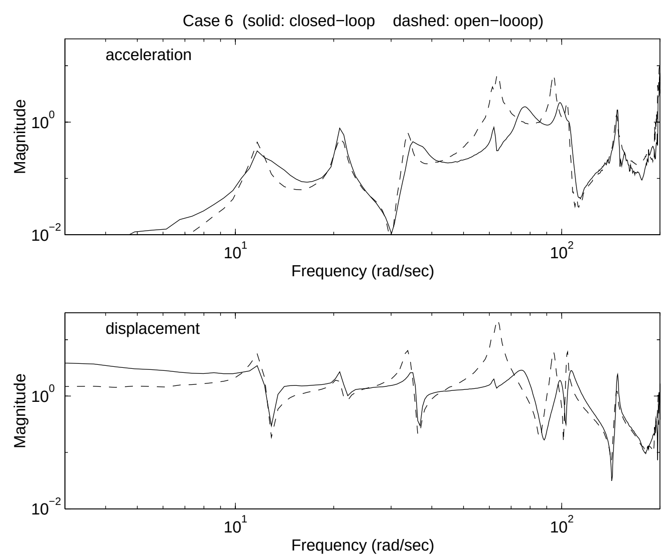

Figure 5.8: Case 6. Frequency response of the transfer functions from actuator 2 to accelerometer 3 and displacement sensor 3. Acceleration is penalized at actuator locations.

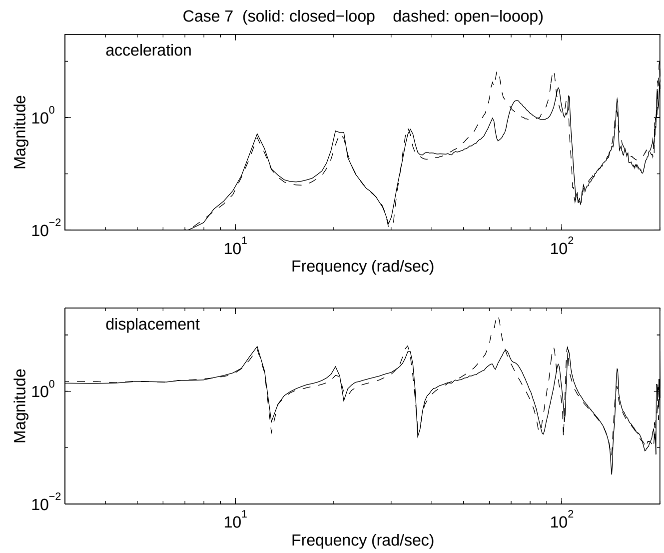

Figure 5.9: Case 7. Frequency response of the transfer functions from actuator 2 to accelerometer 3 and displacement sensor 3. Velocity is penalized at actuator locations using only velocity feedback.

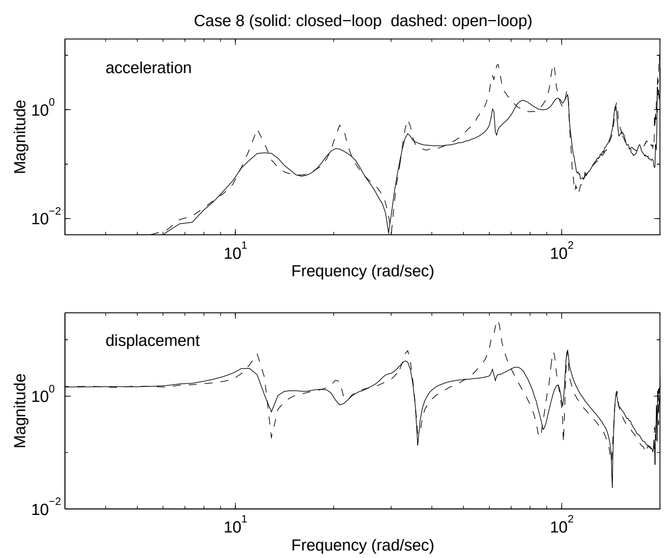

Figure 5.10: Case 8. Frequency response of the transfer functions from actuator 2 to accelerometer 3 and displacement sensor 3. Acceleration is penalized at accelerometer locations using only acceleration feedback.

Chapter 6

Optimal Sensor Placement

Choosing an effective set of sensor measurements is essential for designing controllers to achieve stringent performance and robustness objectives. Often control requirements are not considered in the design stage for physical systems and the location of sensors for control are chosen in an *ad hoc* manner. Flexible structures are especially challenging systems to determine sensor locations and types due to the large number of lightly damped modes to be controlled. Also, tradeoffs need to be considered which balances the number of sensors needed to observe a large number of modes while simultaneously considering the added weight cost and quality of these additional sensors.

One approach to the selection of sensor locations is to consider a cost function which includes the observability grammians in minimizing a cost function. Skelton and DeLorenzo consider a cost function as an LQG performance metric formulated as the root mean square contribution of each sensor output. Sensors associated with small cost functions may be removed due to their low effectiveness [42]. Similar approaches are developed using modal properties. Kim and Jenkins choose a performance metric based on modal controllability weighted by the modal cost of Skelton [26]. This approach emphasizes both the degree of controllability and modal participation in the performance criteria. An alternative approach by Lim involves the relationship between grammian singular values and modal observability [27]. The performance metric is a weighted modal projection with actuator and sensor pairs chosen such that principal directions are parallel to the modes with large singular values. In [7] Balas and Young develop a sensor selection technique that takes into account the closed-loop performance objectives. Different sensor locations are compared based on the information each group of sensors can observe. The information is quantified in terms of the associated H_2 cost of estimating the full system state.

This chapter considers a technique based on Full Control synthesis for choosing a sensor configuration. In this technique it is possible to include the system uncertainties and closed-loop performance objectives into the sensor selection process. The Full Control system allows the controller to independently affect every state and error signal. Computing the optimal Full Control controller is equivalent to computing the optimal controller for a given set of sensors. Synthesis of globally optimal controllers to minimize an $\mathcal{H}_\infty$ or μ upper bound is formulated in the Linear Matrix Inequality (LMI) framework for Full Information feedback and extended here to the dual problem of Full Control synthesis [30, 29, 38, 28].

The configuration of feedback sensors is closely associated with the issue of control design. The optimal closed-loop system requires an optimal configuration of sensors and optimal gains in the compensator. Optimality in only one of these areas will restrict the achievable performance and robustness of the closed-loop system. Utilizing the Full Control system is advantageous for synthesis and analysis of sensor configuration since a Full Control compensator can be computed which is globally optimal. The procedure will not be affected by local minima associated with control synthesis.

The technique presented in this thesis considers a chosen set of sensor locations. Globally optimal Full Control compensators are computed at each of these locations to determine the maximum performance and robustness level achievable. The sensor locations chosen for implementation on the physical system correspond to the sensor locations achieving the best Full Control performance. There is no guarantee that the optimal Full Control sensor locations are equivalent to the optimal sensor locations for a general output feedback controller; however, experiments indicate this technique can choose effective configurations for a physical system.

The proposed approach easily allows a sensor configuration to be determined by considering variations in both type and location of sensors. The plant model used to design controllers for these configurations may be generated from experimental transfer functions or from a computational finite element model. Additionally, choosing actuator configuration using globally optimal Full Information synthesis is a natural extension to this technique.

Sensor configurations are chosen for a flexible structure using the method described in this section. Several sets of sensor locations are considered for feedback measurements to achieve vibration attenuation at different positions on the structure. Globally optimal Full Control compensators are computed to determine the best sensor configuration of the sets. Output feedback controllers are generated and implemented on the experimental structure using feedback from these sensor configurations.

6.1 Optimally Scaled H_∞ Problem

Consider a linear time-invariant plant $P(s)$ mapping the input signals d and u into output signals z and y.

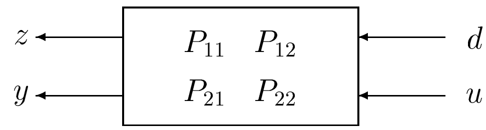

The state space description of $P(s)$ is written as

$$\begin{bmatrix} \dot{x} \\ z \\ y \end{bmatrix} = \begin{bmatrix} A & B_1 & B_2 \\ C_1 & E_{11} & E_{12} \\ C_2 & E_{21} & E_{22} \end{bmatrix} \begin{bmatrix} x \\ d \\ u \end{bmatrix}$$

where $A \in \mathbf{R}^{n\times n}, B_1 \in \mathbf{R}^{n\times n_d}, B_2 \in \mathbf{R}^{n\times n_u}, C_1 \in \mathbf{R}^{n_e\times n}, C_2 \in \mathbf{R}^{n_y\times n}$, and the E matrices of appropriate similar dimensions.

Define $\mathcal{K}_P$ as the set of all real, rational, proper controllers, $K(s)$, which stabilize the closed-loop system. Analyzing performance using the induced $\mathcal{H}_\infty$ norm leads to the following minimization problem for $F_l(P, K)$ which is the linear fractional transformation (LFT) for the lower loop of P closed with the controller K (see Section 2.2).

$$\inf_{K\in\mathcal{K}} \sup_{\omega\in\mathbf{R}} \overline{\sigma}\left[F_l\left(P(\jmath\omega), K(\jmath\omega)\right)\right] \;=\; \inf_{K\in\mathcal{K}} \|F_l\left(P, K\right)\|_\infty$$

This is an H_∞ optimal controller synthesis problem which has been explained briefly in Section 2.2.

In this section the problem of minimizing the scaled H_∞ norm will be explained. Consider the set of scalings defined as

$$\mathcal{D} = \left\{diag\left(D_1^R, \ldots, D_m^R, D_1^C, \ldots, D_n^C, d_1^c I_{c_1}, \ldots, d_p^c I_{c_p}\right)\right.$$

The optimally scaled H_∞ problem is [39, 28]

$$\beta_{opt} = \inf_{\substack{D\in\mathcal{D} \\ K\in\mathcal{K}_P}} \|D^{\frac{1}{2}} F_l(P, K) D^{-\frac{1}{2}}\|_\infty \qquad (6.1.1)$$

Since the uncertainty block Δ and the scaling block D commute the following relations hold

$$F_u(D^{\frac{1}{2}}PD^{\frac{-1}{2}}, \Delta) = F_u(P, \Delta)$$

$$\bar{\sigma}(D^{\frac{1}{2}}PD^{\frac{-1}{2}}) \geq \mu(P)_\Delta$$

Hence, the D scalings provide a way of taking in to account the structure of the uncertainties and the constant β_{opt} in definition 6.1.1 is an upper bound for μ (see section 2.3.

The solution of the scaled H_∞ problem is not convex and an exact solution does not exist [13]. With some simplifications on the problem data however, the optimally scaled H_∞ problem can be cast as a LMI problem which gives a global minimum for β_{opt}. In the next section optimal H_∞ problem will be formulated as a convex LMI problem and full control problem will be explained.

6.2 LMIs and Full Control Problem

The LMI feasibility conditions utilize a matrix T_α which is formulated for a real scalar $\alpha > 0$.

$$T_\alpha = \begin{bmatrix} I & \sqrt{2\alpha}I \\ \sqrt{2\alpha}I & \alpha I \end{bmatrix}$$

This matrix is used to compute the following star product LFT .

$$F_s(T_\alpha, M) = \begin{bmatrix} (I+\alpha A)(I+\alpha A)^{-1} & \sqrt{2\alpha}\,(I+\alpha A)^{-1} B \\ \sqrt{2\alpha}C\,(I+\alpha A)^{-1} & E+\alpha C\,(I+\alpha A)^{-1} B \end{bmatrix}$$

The block diagram for the star product is shown in Figure 6.1

Computing the star product with T_α has several important properties. The most immediately noticed property is the relationship between the star product and the

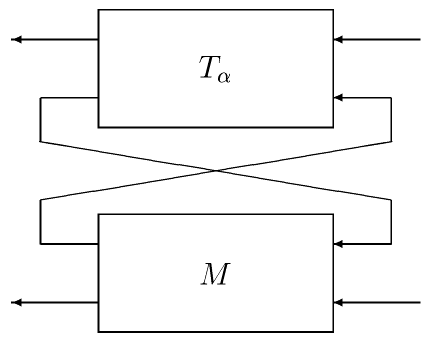

Figure 6.1: Star Product

bilinear transformation. The matrix $\hat{P} = F_s(T_\alpha, P)$ is the discrete-time formulation of the continuous-time plant P. The star product also has a commutation property such that $F_s\left(T_\alpha, F_l(P, K)\right) = F_l(P, F_s(T_\alpha, K))$.

The following theorem demonstrates a constant matrix condition, formulated using the star product, which is equivalent to an $\mathcal{H}_\infty$ condition [39].

Theorem 6.2.1 *Given the state-space plant $P(s)$, its associated constant matrix data M_P, and the set $\mathcal{D}$ of scaling matrices, the following are equivalent.*

1. *There exists $D \in \mathcal{D}$ and stabilizing $K \in \mathcal{K}_P$ such that*

$$\|D^{\frac{1}{2}} F_l(P, K) D^{-\frac{1}{2}}\|_\infty < 1$$

2. *There exists $D \in \mathcal{D}$ and stabilizing $K \in \mathcal{K}_P$ along with real $X = X^T > 0$ such that with $Z = diag(X, D)$,*

$$\overline{\sigma}\left(Z^{\frac{1}{2}} F_s(T_\alpha, F_l(M_P, K)) Z^{-\frac{1}{2}}\right) < 1$$

3. *There exists $D \in \mathcal{D}$ and stabilizing $K \in \mathcal{K}_P$ along with real $X = X^T > 0$ such that with $Z = diag(X, D)$,*

$$\overline{\sigma}\left(Z^{\frac{1}{2}} F_l(F_s(T_\alpha, M_P), K) Z^{-\frac{1}{2}}\right) < 1$$

Now perform a change of variables. Denote $\{R, U, V, T\}$ as elements of the constant matrix term involving the star product $F_s(T_\alpha, M_P)$. Introduce Q to replace $K(I + TK)^{-1}$ in the closed-loop LFT for notational convenience.

$$F_l\left(F_s\left(T_\alpha, M_P\right), K\right) = F_l\left(\begin{bmatrix} R & U \\ V & T \end{bmatrix}, K\right) = R + UQV$$

The final theorem presents the pair of LMI optimizations that represent the $\mathcal{H}_\infty$ controller feasibility condition for a general output feedback system. The variant of Parrott's theorem is applied to the constant matrix condition involving the maximum singular value [40].

Theorem 6.2.2 *Given the state-space plant $P(s)$ and associated constant matrix M_P with the star product elements $F_l\left(F_s\left(T_\alpha, M_P\right), K\right) = R + UQV$ along with the set $\mathcal{D}$ of scaling matrices, then the following are equivalent.*

1. *There exists stabilizing $K \in \mathcal{K}_P$ and $D \in \mathcal{D}$ such that*

$$\|D^{\frac{1}{2}} F_l(P, K) D^{-\frac{1}{2}}\|_\infty < 1$$

2. *There exists stabilizing $K \in \mathcal{K}_P$ and $D \in \mathcal{D}$ along with real $X = X^T > 0$ such that with $Z = diag(X, D)$,*

$$\overline{\sigma}\left(Z^{\frac{1}{2}}(R + UQV)Z^{-\frac{1}{2}}\right) < 1$$

3. *There exists stabilizing $K \in \mathcal{K}_P$ and $D \in \mathcal{D}$ along with real $X = X^T > 0$ such that with $Z = diag(X, D)$,*

$$\overline{\lambda}\left(U_\perp^T\left(RZ^{-1}R^T - Z^{-1}\right)U_\perp\right) < 0$$

$$\overline{\lambda}\left(V_\perp\left(R^T Z R - Z\right)V_\perp^T\right) < 0$$

6.2.1 Full Control Problem

When the state-space representation of the plant P_{fc} is in the special form

$$P_{fc} = \left[\begin{array}{c|cc} A & B & [I \;\; 0] \\ \hline C_1 & E_{11} & [0 \;\; I] \\ C_2 & E_{21} & [0 \;\; 0] \end{array}\right]$$

the controller will have direct access to states and disturbance signal. This special problem is called the full control problem. Define $M_{P_{fc}}$ as the constant matrix associated with the state-space elements of P_{fc}. Formulate the R, U, V elements of the star product term $F_s\left(T_\alpha, M_{P_{fc}}\right)$.

$$R = \begin{bmatrix} (I+\alpha A)(I+\alpha A)^{-1} & \sqrt{2\alpha}\,(I+\alpha A)^{-1} B_1 \\ \sqrt{2\alpha}C_1 (I+\alpha A)^{-1} & E_{11} + \alpha C_1 (I+\alpha A)^{-1} B_1 \end{bmatrix}$$

$$U = \begin{bmatrix} \sqrt{2\alpha}\,(I+\alpha A)^{-1} B_1 & 0 \\ \alpha C_1 (I+\alpha A)^{-1} & I \end{bmatrix}$$

$$V = \begin{bmatrix} \sqrt{2\alpha}C_2 (I+\alpha A)^{-1} & E_{12} + \alpha C_2 (I+\alpha A)^{-1} B_1 \end{bmatrix}$$

The matrix U is square and invertible for the Full Control system. This full rank condition is anticipated by the complete controllability of this system. A linearly independent set of control vectors are available to affect the states and error outputs of the plant. Correspondingly, the perpendicular subspace, $U_\perp$, utilized in the LMI conditions for $\mathcal{H}_\infty$ controller feasibility is null.

The feasibility condition for existence of an $\mathcal{H}_\infty$ controller for Full Control feedback is reduced to a single LMI. The LMI involving $U_\perp$ in Theorem 6.2.2 is vacuous and automatically satisfied. The remaining LMI involving variables V and $V_\perp$ constitutes the only condition for Full Control feasibility as demonstrated in Theorem 6.2.3.

Theorem 6.2.3 *Given the Full Control plant P_{fc} and scaling set $\mathcal{D}$, define the following :*

1. *The augmented scaling matrices $\mathcal{Z}$*

$$\mathcal{Z} = \left\{ \begin{bmatrix} X & 0 \\ 0 & D \end{bmatrix} : 0 < X = X^T \in \mathbf{R}^{n \times n}, D \in \mathcal{D} \right\}$$

2. *Real scalar $\alpha > 0$, so that $(I - \alpha A)$ is invertible*

3. *R and V as defined above*

4. *$V_\perp$ such that $V^T V_\perp = 0$ and $\begin{bmatrix} V \\ V_\perp \end{bmatrix}$ is invertible*

Then, there exists a stabilizing $K \in \mathcal{K}_{P_{fc}}$ and a constant $D \in \mathcal{D}$ such that

$$\left\| D^{\frac{1}{2}} F_l \left(P_{fc}, K \right) D^{-\frac{1}{2}} \right\|_\infty < 1$$

if and only if the following convex set is nonempty.

$$\left\{ Z \in \mathcal{Z} : \lambda_{max} \left[V_\perp \left(R^* Z R - Z \right) V_\perp^* \right] < 0 \right\} \neq \{\emptyset\}$$

6.3 Optimal Sensor Placement for the Flexible Structure

The technique of selecting sensor locations based on full control synthesis is applied to the University of Minnesota flexible structure (Chapter 3). The results in Chapter 5 of this thesis show that accelerometer feedback is more effective than displacement feedback for vibration attenuation and accelerometers provide greater freedom in sensor location selection, hence only optimal placement of accelerometer sensors are considered.

The accelerometers are grouped as follows:

a_3^1, a_3^2, a_3^3 accelerometers in Bay 3

a_4^1, a_4^2, a_4^3 accelerometers in Bay 4

The superscripts designate the side of the flexible structure on which the sensors are located and the accelerometers measure accelerations along the directions parallel to the sides of the triangular plates they are attached to (Fig. 3.1).

Six sensor locations are chosen as the candidate optimal sensor locations. The plant models for these sensor locations are obtained by using the least squares frequency domain identification technique explained in Chapter 4. The nominal sensor locations are shown in Table 6.1. The block diagram for the control problem formulation is shown in Figure 6.2

Location#	*Sensor combination*
1	a_3^1, a_3^2
2	a_3^1, a_3^2, a_3^3
3	a_4^1, a_4^2
4	a_4^1, a_4^2, a_4^3
5	a_3^1, a_4^1
6	a_3^1, a_4^2

Table 6.1: Nominal sensor locations

The additive uncertainty block W_{add} is given as

$$Wadd = 4\frac{s^2 + 72s + 4790}{s^2 + 205s + 28910}$$

The performance objective is to attenuate the bay 3 and bay 4 accelerations. For this, the acceleration measurements are penalized. W_{per} in fig 6.2 represents the performance penalty and given for bay 3 and bay 4 as

$$W_{per}^{bay3} = \frac{4.6}{10} \quad W_{per}^{bay4} = \frac{3.5}{10}$$

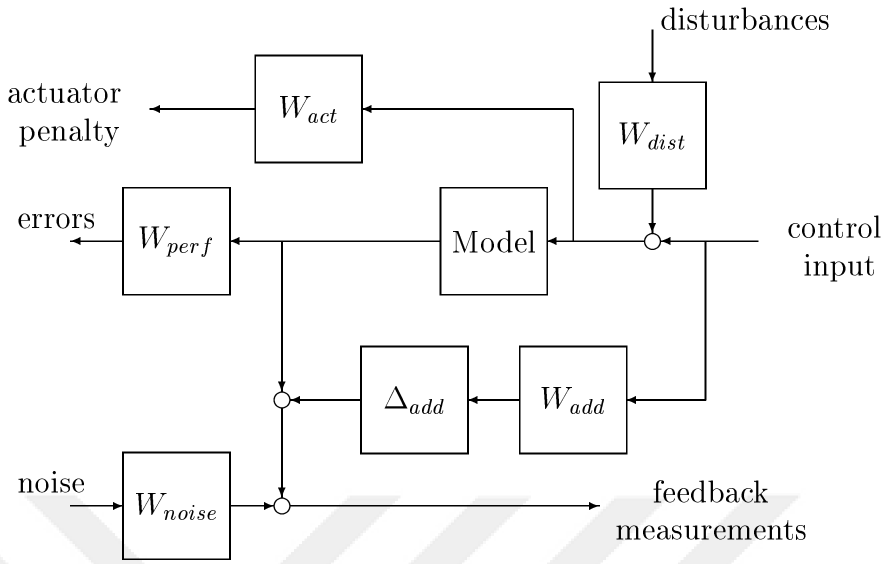

Figure 6.2: Flexible Structure Block Diagram

These performance weights approximately correspond to an attenuation ratio of 4:1 of the largest peak at the frequency range of 10 to 100 rad/sec.

W_{noise} is a diagonal matrix with 0.01 as the diagonal elements. This corresponds to a 1% noise uncertainty on the acceleration measurements. A constant weighting, $W_{dist} = 0.5$, is included to normalize the disturbance signal affecting each actuator. To limit the actuator command signals in the control design process to ± 5 volts ($\pm$3lbs), a value of 1/5 is used to weight each actuator signal. The weight W_{act} is $\frac{1}{5} I_{3\times 3}$.

Full control compensators are computed for the sensor locations in Table 6.1. The error signals to be attenuated are either bay 3 accelerations (a_3^1, a_3^2, a_3^3) or bay 4 accelerometers (a_3^1, a_3^2, a_3^3). The μ performance levels for the optimal Full Control compensators are given in Table 6.2.

The second column of Table 6.2 shows the effectiveness of the six sensor configurations in attenuating the bay 3 accelerations. The most effective sensor configuration

Feedback Accelerometers	bay 3 Performance $\|3_1, 3_2, 3_3\|_\infty$	bay 4 Performance $\|4_1, 4_2, 4_3\|_\infty$
$3_1, 3_2$	1.378	3.031
$3_1, 3_2, 3_3$	0.299	0.719
$4_1, 4_2$	1.641	0.656
$4_1, 4_2, 4_3$	0.299	0.511
$3_1, 4_1$	3.281	1.312
$3_1, 4_2$	1.641	0.609

Table 6.2: Achievable Full Control μ Performance Levels

for bay 3 vibration attenuation is to use three sensors in the same bay. Feedback configurations using all bay 3 sensors or using all bay 4 sensors achieve $\mu = .299$ for Full Control closed-loop performance. These performance levels are similar since the set of sensors in each bay is able to observe the dynamics of bay 3. Each set of accelerometers is able to provide sufficient information to the controller to attenuate the bay 3 vibration responses.

Restricting the feedback to only two sensors significantly decreases the optimal performance level. The μ values increase by approximately a factor of 4 when using $\{3_1, 3_2\}$ as compared to $\{3_1, 3_2, 3_3\}$ for feedback. The performance decreases even more if the two sensor are aligned in the same direction. The μ of 3.28 is for $\{3_1, 4_1\}$ is twice the $\mu = 1.64$ value achieved when using $\{3_1, 4_2\}$. This is due to the fact that one of the bending modes can only be sensed partially with a two sensor configuration.

The results in Table 6.2 are based on Full control design which assumes full authority of the actuators which is not practical. However, the assumption is that the controllers designed by D-K iteration will have similar performance to the full control controllers in terms of preserving the sensor configuration relations. Output feedback controllers are generated using *D-K* iteration for vibration attenuation of the bay 3 accelerometers. Separate controllers are designed for 2 different feedback configurations. The first controller, K_3^3, will use the 3 sensors in bay 3 to control vibration in bay 3. The second controller, K_4^3 will feedback the 3 sensors in bay 4 to attenuate vibration in bay 3.

Robust stability is plotted for each controller in Figure 6.3. The peak robust stability singular values are 0.445 for K_3^3 and 0.456 for K_4^3. μ value is less than one for each controller which indicates that the desired robustness objectives are achieved.

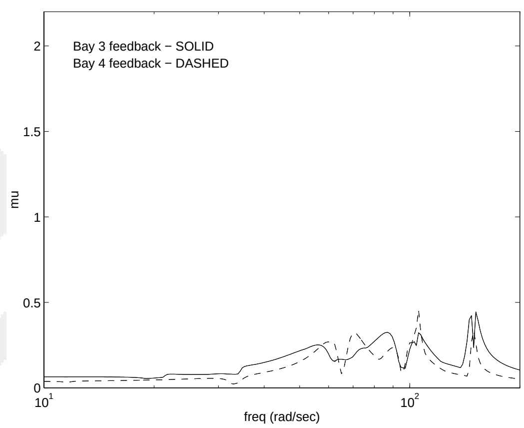

Figure 6.3: Robust Stability

Nominal performance is also calculated for each controller as 1.152 for K_3^3 and 1.880 for K_4^3. The weighted norms greater than 1 indicate neither controller is able to achieve the desired performance objectives. Nominal performance is plotted in Figure 6.4. The robust performance μ values for each controller is given in Figure 6.5. The μ upper bounds are computed as 1.296 for K_3^3 and 2.065 for K_4^3. Each controller gives a peak μ greater than 1 indicating robust performance is not achieved for either output feedback controller.

The robust performance μ plots are of similar shape for each controller with peaks at the modes, though μ for K_4^3 is much higher. Both controllers are driven by meeting the performance goals as evidenced by Figure 6.4.

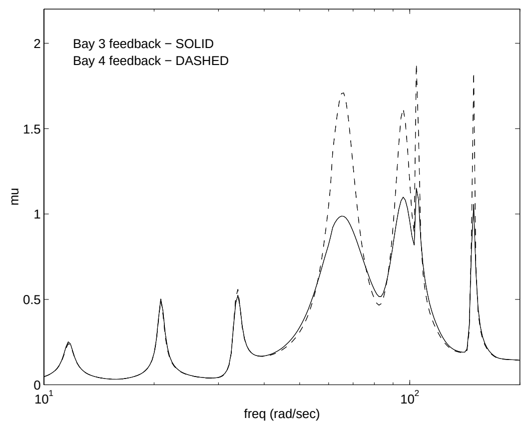

Figure 6.4: Nominal Performance

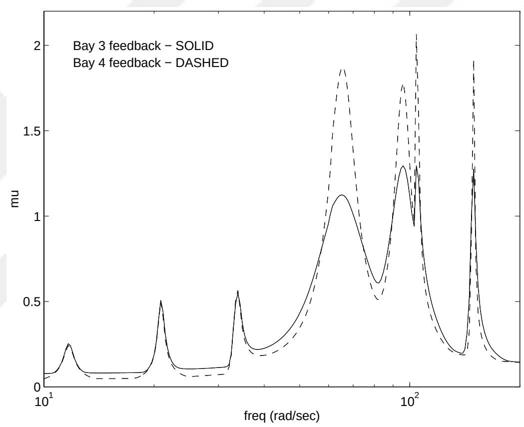

Figure 6.5: μ for Robust Performance

The μ values resulting from full control synthesis indicate that the same performance could be achieved by bay 3 and bay 4 acceleration feedback. The poor performance of the D-K iteration controller K_4^3 may be explained by the fact that the full control results are globally optimal whereas D-K iteration may result in a controller far from the optimal one.

D-K iteration controllers are implemented on the structure (see Section 3). Magnitude plots of the experimental transfer functions from actuator 2 to bay 3 accelerometers are shown in Figure 6.6. K_3^3 provides better attenuation at the mid-frequency range which agrees with the robust performance plot 6.5.

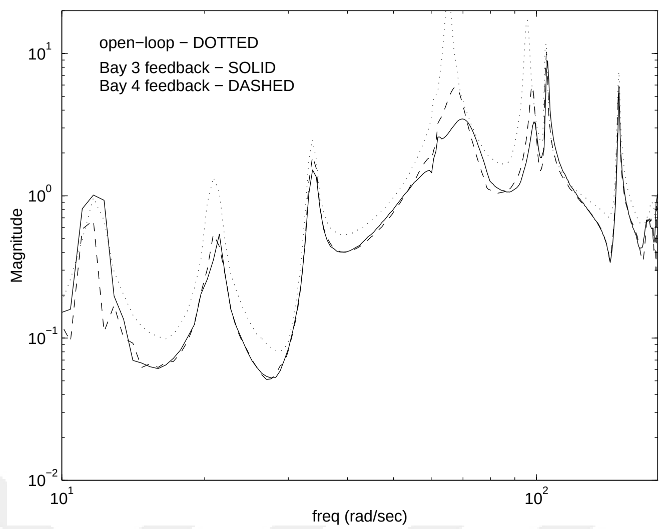

Figure 6.6: Experimental Closed-Loop Peak Gains for bay 3 Accelerometers with K_3^3 (—) and K_4^3 (- - -)

The performances of the optimal full control compensators in attenuating bay 4 accelerations using the same sensor configurations are shown in the third column of Table 6.2. The μ values in Table 6.2 indicate that feedback measurements from bay 4 are necessary for adequate attenuation of bay 4 vibrations. Designing a full control compensator with only two of the bay 3 accelerometers gives a μ value of 3.031 and using all three sensors in bay 3 achieves a μ value of 0.719. Feeding back all three of the bay4 accelerometers achieves a μ value of 0.511.

The need for utilizing bay 4 accelerometers to control bay 4 vibrations can be seen by the open-loop responses in Figure 6.7. A torsional mode exists at 62 *rad/sec* that is clearly observable by bay 4 but does not appear in the frequency response data of bay 3. Any feedback configuration utilizing only bay 3 sensors fails to provide information to the controller about the torsional mode dynamics at this frequency. Consequently, the controller can not adequately effect these dynamics as is demonstrated by the poor closed-loop performance.

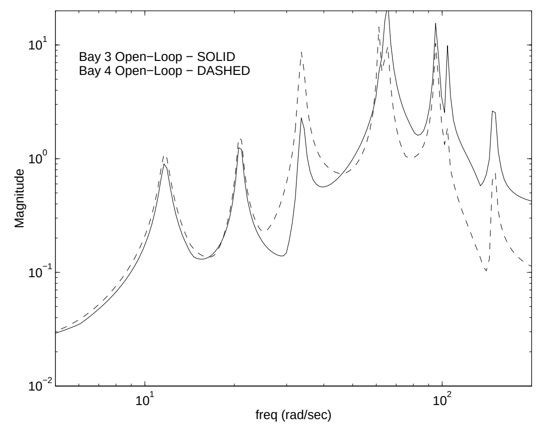

Figure 6.7: Open-Loop Peak Gains from bay 3 Actuators to bay 3 and bay 4 Accelerometers

Two output feedback controllers are synthesized using D-K iteration for vibration attenuation of the bay 4 accelerometers. K_3^4, uses bay 3 accelerometers to control vibration in bay 4. K_4^4, uses bay 4 accelerometers to attenuate vibration in bay 4. Figure 6.8 shows the robust stability plots for bay 4 controllers. K_3^4 and K_4^4 both achieve robust stability with largest singular values of 0.71 and 0.79 respectively.

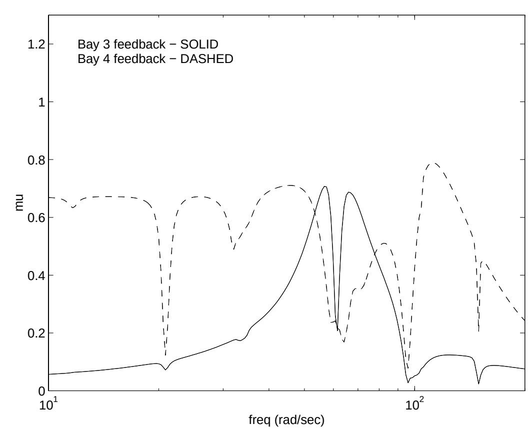

Figure 6.8: Robust Stability

The nominal performance plots are shown in Fig. 6.9. The nominal performance value for K_3^4 is 1.2 and for K_4^4 it is 0.54. A value greater than 1 indicates that performance objectives can not be achieved used only bay 3 accelerations.

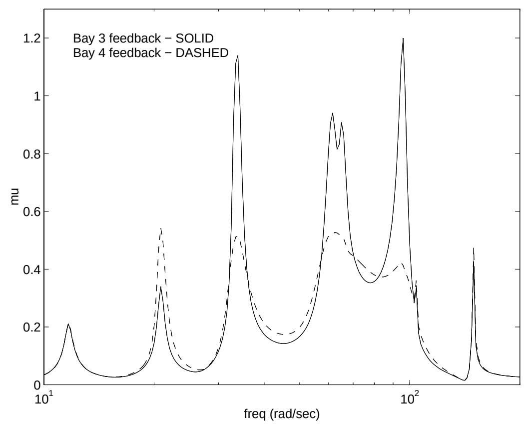

Figure 6.9: Nominal Performance

The robust performance μ values for each controller are given in Figure 6.10. The μ upper bounds are computed as 0.98 for K_4^4 and 1.27 for K_3^4. The controller using bay 4 feedback, K_4^4, is able to achieve robust performance while K_3^4 is unable to achieve the desired robustness goals due to its associated μ being greater than 1.

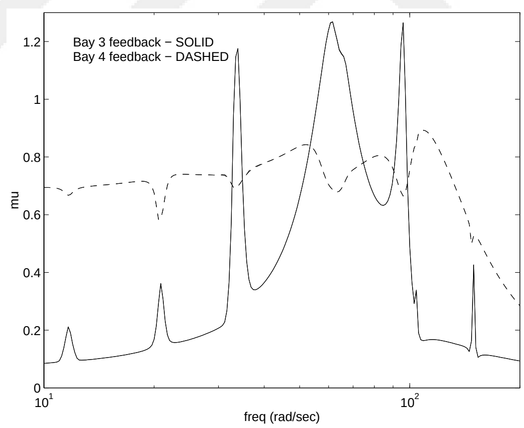

Figure 6.10: μ for Robust Performance

Implementing each controller on the experimental flexible structure produces performance levels which agree with the Full Control synthesis results. Using bay 4 accelerometers as feedback measurements allows better vibration attenuation than using bay 3 feedbacks. Peak gains of closed-loop transfer functions from the experimental flexible structure are presented in Figure 6.11. K_3^4 demonstrates the expected poor performance in attenuating the 62 *rad/sec* mode while K_4^4 is able to attenuate each mode to nearly equal peak gains as expected by the μ plots.

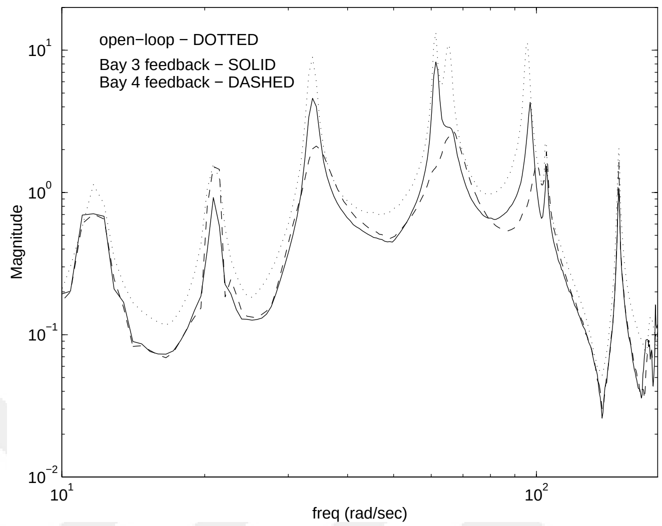

Figure 6.11: Experimental Closed-Loop Peak Gains for bay 4 Accelerometers with K_3^4 (—) and K_4^4 (- - -)

Chapter 7

Summary and Conclusions

In this thesis system identification, performance criteria selection and optimal sensor placement for flexible structures are examined. The ideas developed are tested on an experimental flexible structure.

A system identification technique based on orthonormal basis functions is applied to identify input/output response of the experimental flexible structure. This resulted in identified SISO models for each input/output channel of the data. The a-priori information about the poles of the experimental structure for the orthonormal basis identification is obtained from a classical linear least squares identification technique. A matrix partial fraction expansion method is used to obtain a MIMO state space realization of the experimental structure from individual SISO systems. This model is used to design a high performance vibration attenuation controller using H_∞ control techniques. This controller is implemented on the structure and good agreement is observed between the predicted and experimental performance.

Unlike most of the feedback design problems there usually is a freedom to choose the signals to be penalized and the signals to be fed back in flexible structure control design. The next area of research focused on the selection of error signals and performance weights for active vibration attenuation in flexible structures. It is shown that the controllers may succeed in achieving what is being asked for by the design criteria but this may not be the overall desired result. The choice of performance weightings and the signals being penalized play an extremely important role and they must be selected based on the performance objectives. The type of attenuation desired (acceleration, velocity, displacement at collocated and noncollocated locations) and the frequency range of interest are factors that dictate the choice of penalty weights and error signals as well as sensor locations. Penalizing signals measured at accelerometer locations gave good results. This has the advantage that acceleration measurements are accurate and sensors can be placed anywhere on the structure easily.

The results on performance criteria selection leads to the question of sensor location selection on flexible structures. In the last part of this thesis a technique based on full control design is presented for selecting optimal sensor locations. The technique is optimal in the sense that it selects the best sensor configuration among a given set of sensor locations. Globally optimal Full Control compensators are computed at each of these locations to determine the maximum performance and robustness level achievable. The sensor locations chosen for implementation on the physical system correspond to the sensor locations achieving the best Full Control performance. There is no guarantee that the optimal Full Control sensor locations are equivalent to the optimal sensor locations for a general output feedback controller; however, experiments indicate that this technique can choose effective configurations for a physical system. In this technique model uncertainties and closed-loop performance objectives can easily be incorporated into the sensor placement process.

There are two obvious areas that can be considered as extensions to the research presented in this thesis. The first is to develop a systematic technique for refining the a-priori pole location information necessary for identification with generalized orthonormal basis functions and a quantitative examination of the sensitivity of the identification technique to the errors in pole locations. The second research area is the optimal placement of actuator locations for closed loop control. This problem is dual to optimal sensor placement problem and can be formulated as a Full information synthesis problem. It may also be interesting to formulate the optimal sensor/actuator placement problems so that elements of **B** and **D** matrices of the state space representation are found rather than selecting one location among a given set of locations.

Bibliography

[1] V.M. Adamjan, D.Z. Arov, and M.G. Krein. Infinite block hankel matrices and related extension problems. *AMS Transl*, 111:133–156, 1978.

[2] G. J. Balas. *Robust control of flexible structures: Theory and experiments*. PhD thesis, California Institute of Technology, Pasadena, 1989.

[3] G. J. Balas, J. Doyle, K. Glover, A. Packard, and R. Smith. *μ-analysis and Synthesis Toolbox*. MUSYN Inc. and MATHWORKS Inc., Minneapolis, MN, 1993.

[4] G. J. Balas and J. C. Doyle. Identification for robust control of flexible structures. In *Proceedings of the 1989 American Control Conference*, Pittsburgh, PA, 1989.

[5] G. J. Balas and J. C. Doyle. Robustness and performance trade-offs in control design for flexible structures. *IEEE Transactions on Control Systems Technology*, 2(4):352–361, 1994.

[6] G. J. Balas and P.Young. Control design for variations in structural natural frequencies. *AIAA Journal of Guidance, Control and Dynamics*, 18:325–332, 1995.

[7] G. J. Balas and P. M. Young. Sensor selection via closed-loop control objectives. *IEEE Transactions on Control Systems Technology*, submitted, 1997.

[8] M. Balas. Trends in large space structure control theory: Fondest hopes, wildest dreams. *IEEE Transactions on Automatic Control*, 27(3):522–535, 1982.

[9] D. S. Bayard. High-order wide-band frequency domain identification using composite curve fitting. In *Proceedings of the 1992 American Control Conference*, pages 3181–3185, Chicago, IL, 1992.

[10] D. S. Bayard, F. Y. Hadaegh, Y. Yam, R. E. Scheid, E. Mettler, and M. H. Milman. Frequency domain identification experiment on a large flexible structure. In *Proceedings of the 1989 American Control Conference*, pages 2532–2542, Pittsburgh, PA, 1989.

[11] J. S. Bendat and A. G. Piersol. *Engineering Applications of Correlation and Spectral Analysis.* John Wiley & Sons, 1993.

[12] J. Bokor, L.Gianone, and Z. Szabo. Construction of generalized orthonormal basis in h_2 space. Technical report, Computer and Automation Research Institute HAS, Hungary., 1995.

[13] S. P. Boyd, Laurant El Ghaoui, Eric Feron, and Venkataramanan Balakrishnan. *Linear Matrix Inequalities in System and Control Theory.* SIAM, Philadelphia, 1994.

[14] R.L. Dailey and M.S. Lukich. Mimo transfer function curve fitting using chebyshev polynomials. In *SIAM 35th Anniv. Meeting*, Denver, CO., 1987.

[15] J. Doyle. Analysis of feedback systems with structured uncertainties. *IEE Proceedings, Part D*, 133(2):45–56, March 1982.

[16] J. Doyle, K. Glover, P. Khargoneker, and B. Francis. State space solutions to standard H_2 and H_∞ control problems. *IEEE Transactions on Automatic Control*, 34(8):831–846, 1989.

[17] J. C. Doyle, J. E. Wall, and G. Stein. Performance and robustness analysis for structured uncertainty. In *Proc. IEEE Control Decision Conf.*, pages 629–636, 1982.

[18] T.T. Georgiou. On computation of gap metric. *Syst. and Control Letters*, 11:253–257, 1988.

[19] L. Gianone. *System Identification for Robust Control Using Noncanonical Basis*. PhD thesis, Computer and Automation Research Institute HAS, Hungary, 1996.

[20] K. Gilpin, M. Athans, and J. Bokor. Multivariable identification of the mit interferometer testbed. In *Proceedings of the 1992 American Control Conference*, pages 1263–1267, Chicago, 1992.

[21] G. C. Goodwin and R. L. Payne. *Dynamic System Identification: Experiment Design and Data Analysis*. Academic Press, New York, 1977.

[22] P.S.C. Heuberger, P.M.J. Van den Hof, and O.H. Bosgra. A generalized orthonormal basis for dynamical systems. *IEEE Trans. Aut. Control*, 40:451–465, 1995.

[23] B. L. Ho and R. E. Kalman. Effective construction of linear state-variable models from input/output functions. *Regelungstechnik*, 14:545–548, 1966.

[24] Jer-Nan Juang. *Applied System Identification*. Prentice-Hall, Englewood Cliffs, New Jersey, 1994.

[25] R. E. Kalman. Irreducable ralizations and degree of a rational matrix. *Journal of SIAM*, 13, 1965.

[26] Y. Kim and J. Junkins. A measure of controllability for actuator placement. *AIAA Journal of Guidance, Control and Dynamics*, 14(5):895–902, 1991.

[27] K. Lims. A method for optimal actuator and sensor placement for large flexible structures. *AIAA Journal of Guidance, Control and Dynamics*, 15(1):49–57, 1992.

[28] R. Lind. *Linear matrix inequalities for robust control: Theory, Algorithms, and Applications*. PhD thesis, University of Minnesota, 1995.

[29] R. Lind, G. J. Balas, and A. Packard. Optimal scaled h_{infty} full information synthesis with real parametric uncertainty. In *Proc. Amer. Control Conf.*, pages 3463–3467. IEEE, 1995.

[30] R. Lind, V. Nalbantoğlu, and G. J. Balas. Choosing sensor configuration for a flexible structure using full control synthesis. In *AIAA Guidance, Navigation and Control Conference AIAA-97-3745*, New Orleans LA, 1997.

[31] J. Little and L. Shure. *Signal Processing Tollbox*. The MATHWORKS Inc., South Natica, MA, 1988.

[32] L. Ljung. *System Identification, Theory for the User*. Prentice-Hall, Englewood Cliffs, New Jersey, 1987.

[33] V. Nalbantoğlu, G. J. Balas, and P. Thomson. The role of performance criteria selection in the control of flexible structures. In *AIAA Guidance, Navigation, and Control Conference, San Diego, CA*, pages 1–9, 1996.

[34] V. Nalbantoğlu, J. Bokor, and G. J. Balas. System identification with generalized orthonormal basis functions: An application to flexible structures. In *2nd IFAC Symposium on Robust Control Design, Budapest, Hungary*, 1997.

[35] D. E. Newland. *An Introduction to Random Vibrations, Spectral and Wavelet Analysis*. Wiley, 1993.

[36] B. Ninnes and F. Gustafson. A unifying construction of orthonormal basis for system identification. Technical Report EE9433, Department of Electrical and Computer Engineering, University of Newcastle, Callaghan 2308, Australia., 1994.

[37] J. P. Norton. *An Introduction to Identifiction.* Academic Press, 1986.

[38] A. Packard, K. Zhou, Pandey, and G. Becker. A collection of robust control problems leading to lmi's. *Proc. 30th IEEE Conference on Decision and Control*, pages 1245–1250, 1991.

[39] A. Packard, K. Zhou, P. Pandey, J. Leonhardson, and G.J. Balas. Optimal, constant I/O similarity scaling for full-information and state-feedback control problems. *Syst. and Control Letters*, 19:271–280, 1992.

[40] S. Parrott. On a quotent norm and the sz.- nagy-foias lifting theorem. *Journal of Functional Analysis*, 30:311–328, 1978.

[41] M. Rosenblum and J Rovnyak. *Hardy Classes and Operator Theory.* Oxford University Press, 1985.

[42] R. E. Skelton and M. DeLorenzo. Space structure control design by variance assignment. *AIAA Journal of Guidance, Control and Dynamics*, 8(4), 1985.

[43] B.F. Spencer, S.J. Dyke, M.K. Sain, and P. Quast. Magnetorheological dampers: a new semi-active control device for seismic response reduction. In *Proceedings of the First European Conference on Structural Control*, Barcelona, Spain, 1996.

[44] S.Toffner-Clausen. *System Identification and Robust Control.* Springer-Verlag, New York, 1996.

[45] P. Stoica and R.L. Moses. *Introduction to Spectral Analysis.* Prentice Hall, 1997.

[46] Z. Szabo, J. Bokor, and F. Schipp. Nonlinear rational approximation using generalized orthonormal basis. In *CDC*, 1997.

[47] A. Tannenbaum. Modified nevanlinna-pick interpolation of linear plants with uncettainty in the gain factor. *International Journal of Control*, 36:331–336, 1982.

[48] P. Thomson, V. Nalbantoglu, and G.J. Balas. Benefits of passive sma elements in active vibration control. In *Proceedings of the First European Conference on Structural Control*, Barcelona, Spain, 1996.

[49] P.M.C. Van den Hof, P.S.C. Hueberger, and J. Bokor. System identification with orthonormal basis functions. *Automatica*, 31, 1995.

[50] B. Wahlberg. Identification of resonant systems using kautz filters. *Proc. 30th IEEE Conference on Decision and Control*, pages 2005–2010, 1991.

[51] B. Wahlberg. System identification using laguerre models. *IEEE Trans. Automatic Control*, 36:551–562, 1991.

[52] B. Wahlberg and M. Makila. On approximation of stable linear dynamical systems using laguerre and kautz functions. *Automatica*, 32:693–708, 1996.

[53] G. Wolodkin, V. Nalbantoglu, K.B. Lim, and G.J. Balas. Application of parametric uncertainty modeling to a flexible structure. In *Proceedings of DETC'97 1997 ASME Design Engineering Technical Conferences*, Sacramento, CA, 1997.

[54] G. Zames. Optimal sensitivity and feedback: Weighted seminorms, approximate inverses and plant invariant schemes. In *Proc. Allerton Conf.*, 1979.

[55] G. Zames. Feedback and optimal sensitivity: Model reference transformation, multiplicative seminorms, and approximate inverses. *IEEE Transactions on Automatic Control*, 26:301–320, 1981.

[56] G. Zames and El-Sakkary. Unstable systems and feedback: The gap metric. In *Proc. Allerton Conf.*, pages 380–385, 1980.

[57] G. Zames and B. Francis. Feedback, minimax sensitivity, and optimal robustness. *IEEE Transactions on Automatic Control*, 28:585–600, 1983.

[58] K. Zhou, J.C. Doyle, and K. Glover. *Robust and optimal control.* Prentice Hall, New Jersey, 1996.